JBC RESEARCH ARTICLE

Heat shock protein Hspa13 regulates endoplasmic reticulum and cytosolic proteostasis through modulation of protein translocation

Received for publication, May 19, 2022, and in revised form, September 29, 2022 Published, Papers in Press, October 14, 2022,
https://doi.org/10.1016/j.jbc.2022.102597

Mateo F. Espinoza[1,‡], Khanh K. Nguyen[2,‡], Melody M. Sycks[2], Ziqi Lyu[2], Guy M. Quanrud[2], Maureen R. Montoya[2], and Joseph C. Genereux[1,2,*]

From the [1]Graduate Program in Microbiology, and [2]Department of Chemistry, University of California, Riverside, California, USA

Edited by Ursula Jakob

Most eukaryotic secretory proteins are cotranslationally translocated through Sec61 into the endoplasmic reticulum (ER). Because these proteins have evolved to fold in the ER, their mistargeting is associated with toxicity. Genetic experiments have implicated the ER heat shock protein 70 (Hsp70) Hspa13/STCH as involved in processing of nascent secretory proteins. Herein, we evaluate the role of Hspa13 in protein import and the maintenance of cellular proteostasis in human cells, primarily using the human embryonic kidney 293T cell line. We find that Hspa13 interacts primarily with the Sec61 translocon and its associated factors. Hspa13 overexpression inhibits translocation of the secreted protein transthyretin, leading to accumulation and aggregation of immature transthyretin in the cytosol. ATPase-inactive mutants of Hspa13 further inhibit translocation and maturation of secretory proteins. While Hspa13 overexpression inhibits cell growth and ER quality control, we demonstrate that *HSPA13* knockout destabilizes proteostasis and increases sensitivity to ER disruption. Thus, we propose that Hspa13 regulates import through the translocon to maintain both ER and cytosolic protein homeostasis. The raw mass spectrometry data associated with this article have been deposited in the PRIDE archive and can be accessed at PXD033498.

Eukaryotic secretory proteins are primarily targeted to the endoplasmic reticulum (ER), where they fold, mature, and are trafficked to downstream environments (1). This targeting is achieved through N-terminal signal peptides or transmembrane domains (2). Proper targeting of secretory proteins to the ER promotes cellular fitness for two reasons. First, mistargeted protein deprives the organelle of its protein complement. Second, secretory proteins have evolved to mature and fold in the ER (3, 4). Signal peptidases, N-linked glycotransferases, disulfide isomerases, and other ER-localized proteostasis factors are absent from the cytosol. Without these factors, mistargeted secretory proteins cannot be properly processed and hence are prone to aggregation and toxicity. To ensure adequate quality control, multiple mechanisms and checkpoints promote targeting of signal peptide–containing proteins to the ER, primarily through engagement of the ribosome by the signal recognition particle (SRP) and subsequent cotranslational translocation (5, 6). Some proteins, primarily those too short to engage SRP prior to synthesis, are delivered to the translocon through post-translational translocation (7, 8). Proteins that persistently mistarget, for example because of weak signal sequences or cellular stress, are recognized by degradation pathways (9, 10).

The primary protein component of the eukaryotic translocon is Sec61, which is composed of three subunits (α1, β, and γ) (11). A series of associated proteins further support protein translocation. For example, the primary ER heat shock protein 70 (Hsp70) binding immunoglobulin protein (BiP) prevents protein misfolding during translocation, provides ratcheting to prevent backsliding, and is particularly important in assisting translocation for proteins harboring weak signal sequences (12, 13). The J-domain proteins Sec62 and Sec63 stimulate BiP ATPase function, and knockout studies suggest that they are particularly important for post-translational translocation (14–16). The oligosaccharyltransferase (OST) complexes promote cotranslational and post-translational transfer of high mannose glycans onto asparagine in N-linked glycosylation sequons (17, 18). Several literature reports over the past decade suggest that the poorly studied ER Hsp70 Hspa13/STCH might also be involved in protein import. First, Hspa13 localizes to the ER translocon Sec61, based on proximity labeling experiments (19). Hspa13 knockout sensitizes HCT116 human cells to the signal peptidase inhibitor cavinafungin, even more so than signal peptidase components, suggesting a role for Hspa13 in nascent protein maturation (20). Hspa13 expression is negatively associated with mouse life span following prion infection (21). Prion mislocalization to the cytosol, for example because of weak signal sequence, is associated with pathogenicity (22–24). These findings were intriguing, given how little is known about Hspa13 function.

Hsp70 proteins are hub chaperones in the Hsp70 ATP-dependent chaperoning pathway and are present in most cellular compartments (25). As a chaperone, Hsp70 segregates unfolded proteins, preventing inappropriate interactions with other proteins while also promoting folding into the proper conformation (26–28). Unlike other Hsp70s, Hspa13 lacks the

‡ These authors contributed equally to this work.
* For correspondence: Joseph C. Genereux, joeygenereux@gmail.com.

substrate-binding domain (SBD) necessary for canonical Hsp70 functions (Fig. 1*A*) (29, 30). The nucleotide-binding domain (NBD) has 39% identity with both BiP and the cytosolic Hsp70 HSPA1A, and Hspa13 is highly conserved across Eumetazoa (30, 31). Hspa13 is also a target of the unfolded protein response (UPR), selectively induced by the X-box binding protein 1s (XBP1s) arm of the UPR (32, 33). It lacks a KDEL retention motif, leading to its stress-responsive secretion. Finally, reports have implicated Hspa13 in gastric cancer (34, 35), ER-associated degradation (ERAD) (36), plasma cell differentiation (37, 38), and inhibition of programmed cell death (39). However, none of these reports has identified a molecular role for Hspa13.

Herein, we evaluate whether Hspa13 affects secretory protein import into the ER in human embryonic kidney 239T (HEK239T) cells. We find that Hspa13 overexpression inhibits translocation and that ATPase-inhibiting mutations in Hspa13 exacerbate this effect. Inhibited translocation decreases protein secretion, inhibits maturation for the population that still translocates, and leads to the accumulation of mistargeted and aggregated protein in the cytosol. Hence, we find that

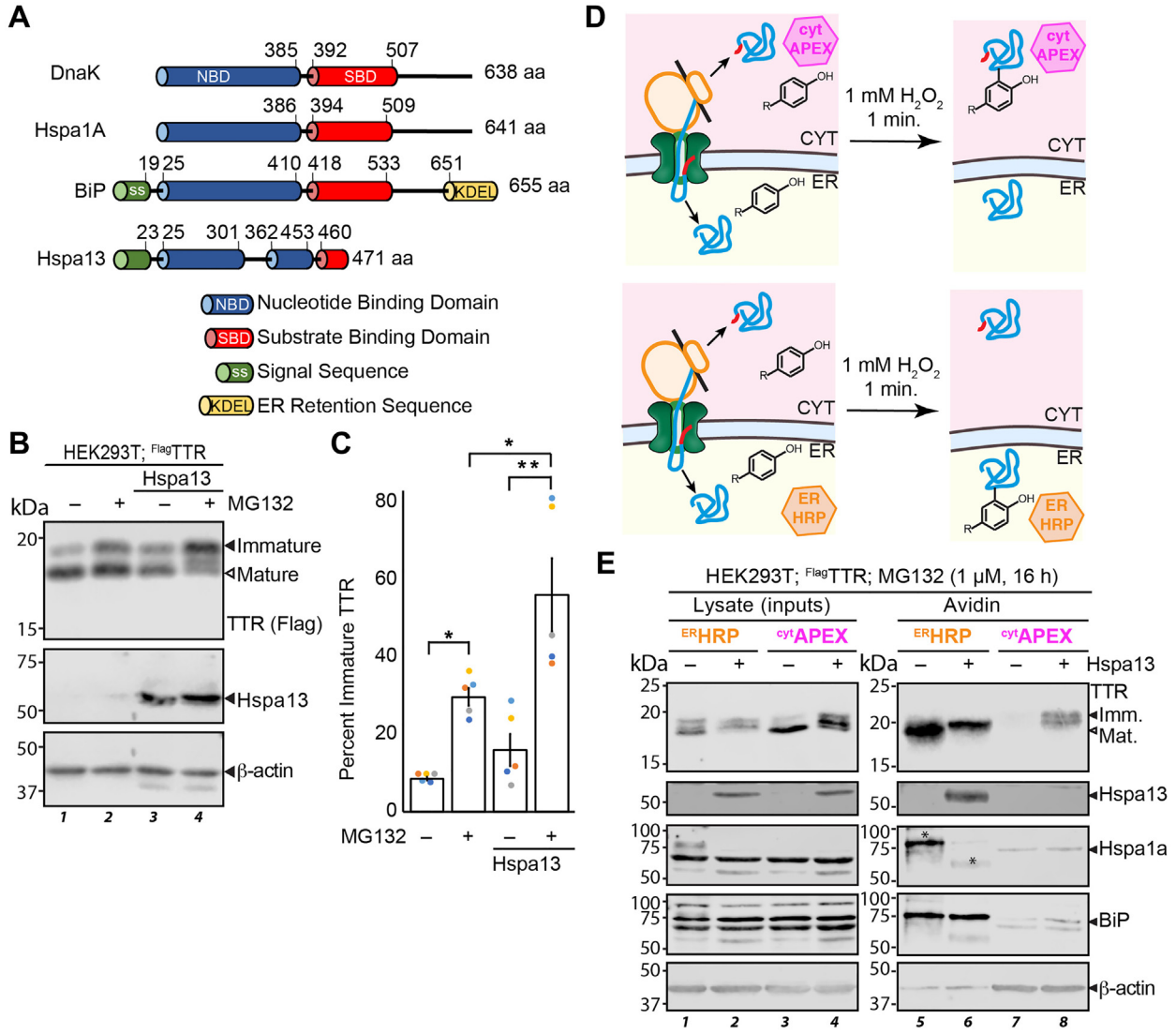

Figure 1. Hspa13 overexpression inhibits TTR import into the ER. *A*, schematic comparing the domain structure of Hspa13 with those of the cytosolic human Hsp70 Hspa1a, the ER human Hsp70 BiP, and the *Escherichia coli* Hsp70 DnaK. *B*, representative immunoblot (n = 5) of SDS-PAGE separated lysates collected from HEK293T cells transiently co-overexpressing ^{FLAG}TTR and Hspa13 as indicated. Cells were treated with either vehicle (0.1% DMSO) or 1 μM MG132 for 16 h prior to lysis. Molecular weight ladders are indicated on the *left* in kilodalton. *C*, bar graph quantifying densitometry from *B*. Percent immature TTR is determined as 100% × the ratio between the upper immature TTR band to the total monomeric TTR signal (n = 5; $^{**}p < 0.01$; $^{*}p < 0.05$). Signal ratios were analyzed using ANOVA ($F = 15.44 > F_{crit} = 3.24$) and then tested for significance with Tukey's HSD test. Error bars represent standard error of the mean. *D*, schematic illustrating the use of proximity labeling peroxidases to identify the ER and cytosolic proteomes. ^{cyt}APEX is an engineered soybean ascorbate peroxidase, whereas HRP is an ER-directed horseradish peroxidase. *E*, representative immunoblot of SDS-PAGE separated lysates from HEK293T cells overexpressing ^{Flag}TTR and Hspa13 as indicated and either ^{ER}HRP or ^{cyt}APEX. Cells were treated with biotin–phenol (BP; 30 min preharvest) and H_2O_2 (1 min preharvest), quenched, and the biotinylated protein purified from lysate using avidin beads. All cells were treated with 1 μM MG132 for 16 h prior to lysis. Hspa1a in lane 5 is obscured by interference from the TTR blotting step, marked with a *, as shown in Fig. S8. APEX, ascorbate peroxidase; BiP, binding immunoglobulin protein; DMSO, dimethyl sulfoxide; ER, endoplasmic reticulum; ^{FLAG}TTR, Flag-tagged TTR; HEK293T, human embryonic kidney 239T cell line; HSD, honestly significant difference; TTR, transthyretin.

modulating Hspa13 abundance and activity leads to imbalances in cytosolic and secretory proteostasis.

Results

Hspa13 overexpression inhibits transthyretin import into the ER

Transthyretin (TTR) is a homotetrameric secretory protein that is frequently used as a model substrate for ER protein homeostasis studies because of its extraordinarily well-characterized biophysical parameters, high secretory load, and disease relevance (40–42). TTR is particularly well suited to ER import experiments, as a small population basally mistargets to the cytosol, this population increases with ER stress, and the immature and mature forms are readily separable by SDS-PAGE gel (43–46). To determine whether Hspa13 affects TTR localization, we co-transfected HEK293T cells with Hspa13 and Flag-tagged TTR (^{Flag}TTR), with the Flag tag immediately C-terminal to the TTR signal peptide. Two TTR bands are apparent at 18 and 16 kDa, consistent with the size of immature and mature ^{Flag}TTR, respectively (Fig. 1*B*). The upper band is less intense, implying that a majority of TTR present in the cell at steady state has had the signal peptide cleaved. TTR contains a cryptic sequon that allows N-glycosylation of misfolded protein (47); however, the bands fail to resolve upon treatment with the deglycosylase PNGase F (Fig. S1*A*), indicating that the upper band represents immature ^{Flag}TTR and not glycosylated protein. Hspa13 overexpression increases the abundance of immature ^{Flag}TTR 1.9 ± 0.5 fold relative to the mature form (Fig. 1, *B* and *C*, lane 1 *versus* lane 3), consistent with ER import inhibition. Mistargeted secretory proteins are subject to degradation (9, 44). Cellular incubation with the proteasomal inhibitor MG132 for 16 h increases total TTR both with and without Hspa13 overexpression (Fig. S1*B*). In the presence of MG132, more immature TTR is observed, with Hspa13 overexpression still increasing immature ^{Flag}TTR by 1.9 ± 0.2 fold. In addition, a small intermediate band appears between the mature and immature forms; we have not yet identified the nature of this species. In summary, if the immature band is indeed cytosolic, these results suggest that Hspa13 inhibits TTR import into the ER.

To better determine the localization of ^{Flag}TTR proteoforms, we performed microsomal separation using digitonin, which selectively lyses the plasma membrane while leaving microsomes intact (Fig. S1*C*). After microsomes are separated from the cytosol through precipitation, fractions are analyzed to determine protein distribution between two subcellular environments (48). We analyzed protein localization in HEK293T cells across a gradient of digitonin concentration. As expected, BiP is present in microsomal pellets (Fig. S1*D*) at all but the highest digitonin concentration. Overexpressed Hspa13 is also detectable in the pellet, confirming its ER localization. However, the ^{Flag}TTR monomers fractionate differently. While mature ^{Flag}TTR cofractionates with the ER proteins, immature ^{Flag}TTR is preferentially (but not solely) found in the supernatant (Fig. S1*D*). Furthermore, while Hspa13 overexpression changes the relative amount of the two ^{Flag}TTR populations (Fig. S1*D*), it does not affect their recovery with digitonin, indicating that Hspa13 impacts ^{Flag}TTR localization in a manner dependent on signal peptide cleavage.

The digitonin assay can determine whether a homogenous population is a better fit between microsomal and cytosolic populations but cannot as readily be used to differentiate whether a protein isoform is partitioned between two locations. Also, this assay copurifies cytosolic aggregates with the microsomal population (49). To better support cytosolic assignment for immature ^{Flag}TTR, we applied our recently reported assay, which uses proximity labeling to measure ER protein mistargeting (46). Specifically, horseradish peroxidase (HRP) with an N-terminal preimmunoglobulin signal sequence and C-terminal KDEL ER retention sequence (^{ER}HRP) localizes to the ER (50), whereas an optimized ascorbate peroxidase (^{cyt}APEX) localizes to the cytosol (51). Cells are incubated with biotin–phenol, which distributes through the cell within 30 min (Fig. 1*D*). Hydrogen peroxide is added, stimulating enzymatic production of biotin–phenoxy radicals that label endogenous proteins within a few nanometers of the peroxidases. Radical quenchers are added after 1 min to minimize off-compartment labeling. Biotinylated proteins are enriched by avidin beads and quantified by Western blotting. The relative labeling of ER and secretory proteins by ^{ER}HRP and ^{cyt}APEX2 then indicates the extent of proper import as opposed to cytosolic mistargeting. As expected, ER resident proteins BiP and Hspa13 are preferentially labeled by ^{ER}HRP, whereas cytosolic β-actin and Hspa1a are selectively labeled by ^{cyt}APEX2 (Fig. 1*E*). In the absence of Hspa13 overexpression, TTR is only labeled by ^{ER}HRP and not by ^{cyt}APEX2. Overexpression of Hspa13 increases the ^{Flag}TTR that is labeled by ^{cyt}APEX2. The migration of this cytosolic TTR is also consistent with that of the immature protein. Hence, Hspa13 inhibits ^{Flag}TTR import and prevents its exposure to signal peptidase.

TTR is a known substrate of pre-emptive quality control, whereby activation of the UPR inhibits protein import into the cytosol (44). If Hspa13 overexpression activates the UPR, pre-emptive quality control could explain consequent ^{Flag}TTR mistargeting. In contrast to Hyou1, whose overexpression robustly increases expression of the UPR target protein BiP, Hspa13 overexpression does not upregulate BiP, indicating that Hspa13 overexpression does not activate the UPR (Fig. S1*E*). Another possibility is that Hspa13 inhibits signal peptide cleavage directly, with immature ^{Flag}TTR then being rapidly retrotranslocated to the cytosol through ERAD. However, we have previously demonstrated that the inhibition of TTR signal peptide cleavage in the ER does not induce its cytosolic accumulation (46) but rather leads to ER accumulation of immature TTR instead.

Hspa13 interacts with multiple components associated with the ER translocon

Hspa13 might inhibit ER TTR import through direct interactions with translocon components. To determine Hspa13 interactors, we employed affinity purification followed by mass

spectrometry (MS). We prepared Hspa13 with a C-terminal Flag (Hspa13^{Flag}). We verified that Hspa13^{Flag} overexpression relocalizes ^{Flag}TTR to the insoluble fraction similarly to untagged Hspa13 overexpression using ultracentrifugation (Fig. S2*A*). Since regulatory interactions are often transient (52), we crosslinked cells with the cell-permeable crosslinker dithiobis(succinimidyl propionate) (DSP) prior to lysis and immunopurification. The crosslinking conditions were optimized to maximize recovery of the known Hspa13 and Sec61 interactor Bcap31 (37, 53) (Fig. S2*B*). We found maximal Bcap31 recovery with 2 mM DSP treatment for 30 min, with only moderate background protein recovery from mock-transfected cells, as determined by silver stain (Fig. S2*C*). Because of concerns over excessive protein loss, however, we limited DSP to 1 mM for the following experiment. Three plates of HEK293T cells were transfected with a mock plasmid (expressing enhanced GFP [eGFP]), and three plates were transfected with Hspa13^{Flag}. Two days post-transfection, cells were crosslinked, the crosslinking quenched, the cells lysed, the lysates normalized to total protein content, and those lysates immunoprecipitated over M2 anti-Flag Dynabeads. The beads were stringently washed with radioimmunoprecipitation assay (RIPA) buffer (50 mM Tris [pH 7.4], 150 mM NaCl, 1% Triton X-100, 0.5% sodium deoxycholate, and 0.1% SDS). Eluted proteins were processed for MS, labeled with tandem mass tags (TMTs), and quantified by MuDPIT shotgun proteomics (Fig. 2*A*). After filtering for common contaminants, 1298 proteins were identified. About 1103 significant interactors were identified by using a previously reported method for correlating recovered protein levels to bait (Hspa13) levels (54), followed by significance testing with Storey's modification of the Benjamini–Hochberg method to a 5% false discovery rate (FDR) (55, 56) (Fig. 2*B* and Table S1).

Hspa13 enrichment from Hspa13^{Flag} cells as compared with mock cells was 47.5 ± 4.1 fold, much lower than the theoretical ratio (∞) but consistent with the ratio compression often seen in TMT-MS2 experiments (57). Interactors include translocon components Sec61a1, Sec61b, NCLN, Sec62, and Sec63, as well as the signal particle recognition receptor component SRPRB and the translocon unclogger ZMPSTE24 (58, 59). Four of five components of the translocon-associated signal peptidase complex (SEC11C, SEC11A, SPCS2, and SPCS3) interact with Hspa13, as do seven of the 12 components of the OST complexes: RPN1, RPN2, DAD1, DDOST, MAGT1, STT3A, and STT3B (60). Although STT3B/MAGT1-containing OST complexes do not associate as strongly with the mammalian translocon, these complexes can still act cotranslationally (17). We do not see association with members of the TRAP complex, which assists with translocation of transmembrane proteins and soluble proteins with a weak signal sequence (61–63). We do not see some reported cytosolic interactors, such as UBQLN2 (64, 65). It could be that our strong washing conditions prevent association with proteins that do not crosslink with Hspa13 in the ER. Another 11 interactors are major ER chaperones (*i.e.*, BiP, ERdj3/DNAJB11, Grp94/HSPB90B1, HYOU1, Hsp47/Erp29, calnexin, PPIB, GANAB, PDIA3, PDIA4), many of which

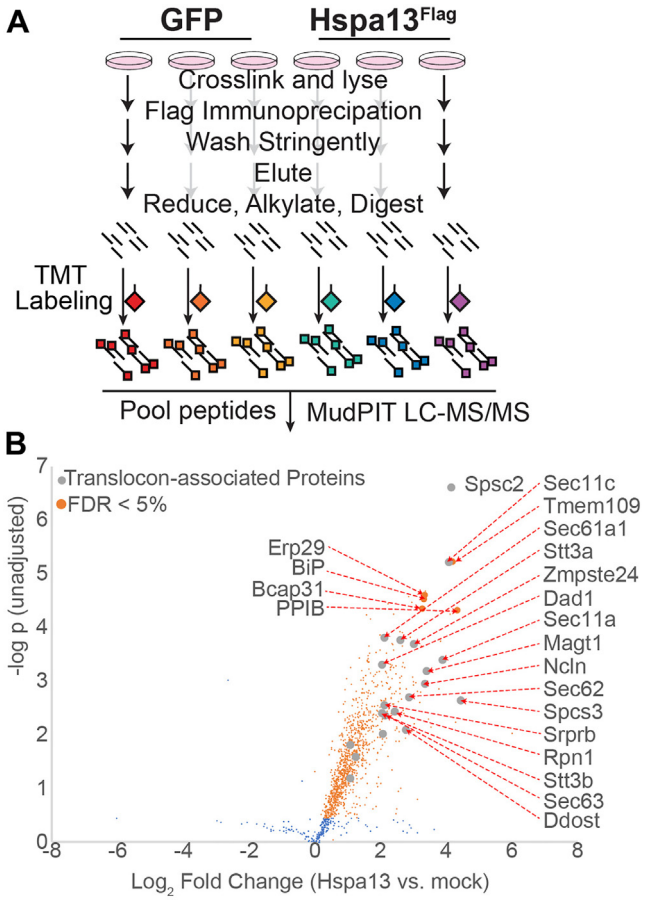

Figure 2. Hspa13 interacts with translocon-associated proteins. *A*, schematic of immunoprecipitation and mass spectrometry (MS) to identify Hspa13 interactors. HEK293T cells overexpressing either mock (GFP) or Hspa13^{Flag} were crosslinked (1 mM DSP for 30 min), crosslinking quenched with 100 mM Tris, and the cells lysed. Lysates were anti-Flag immunoprecipitated, and eluates were processed for MS with tandem mass tag (TMT) labeling. *B*, volcano plot for the relative co-IP recovery of proteins from HEK293T cells overexpressing Hspa13^{Flag} *versus* mock. *Orange dots* correspond to the set of proteins with *q* values (see Experimental procedures section for data analysis) below the false discovery rate threshold of 5%. Co-IP, coimmunoprecipitation; DSP, dithiobis(succinimidyl propionate); HEK293T, human embryonic kidney 239T cell line.

associate with nascent proteins to promote folding and prevent misfolding (66, 67). Several of these chaperones interact with BiP through direct interaction with the NBD (68, 69), which is similar to Hspa13. Hence, the interaction network of Hspa13 is consistent with close association with the translocon and other components involved in maintaining proteostasis for nascent proteins.

Mistargeted ^{Flag}TTR is slowly degraded

Mistargeted secretory proteins can be degraded by the ubiquitin proteasome system (4, 9, 10) or recruited into aggregates (70). We employed a cycloheximide chase to characterize the degradation of ^{Flag}TTR after Hspa13-induced mistargeting (Fig. 3*A*). Cycloheximide arrests protein translation, so that existing populations of protein can be chased over time to determine their clearance kinetics. At the beginning of the chase, the relative proportion of immature

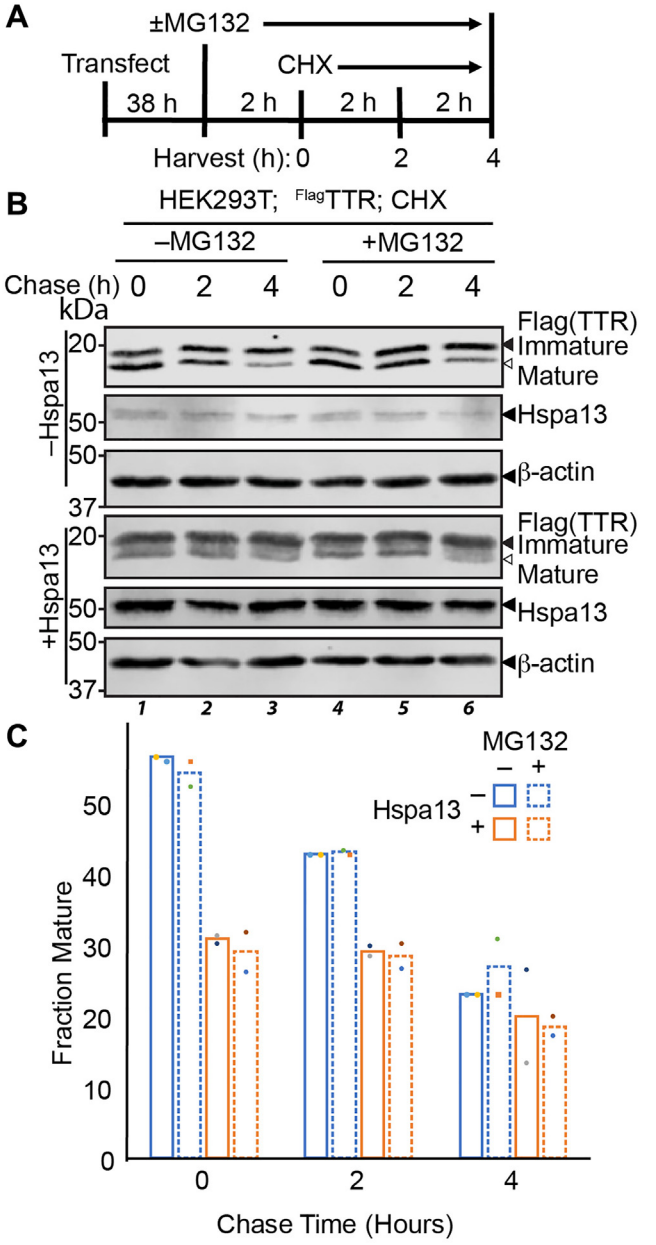

Figure 3. Immature TTR is slowly degraded. *A*, schematic describing the time line of the cycloheximide (CHX) chase experiment. Cells are treated with 10 μM MG132 or vehicle 2 h prior to the chase. The chase is initiated with 50 μg/ml CHX. Cells are harvested and lysed at indicated time points. *B*, representative immunoblot of SDS-PAGE separated lysates from HEK293T cells overexpressing ^{Flag}TTR and Hspa13 treated as indicated. *C*, densitometric quantifications of the fraction of mature TTR during the chase (n = 2). Error bars represent standard deviation. ^{Flag}TTR, Flag-tagged TTR; TTR, transthyretin.

protein is unaffected by the presence of MG132, suggesting that 2 h of proteasomal inhibition is not adequate to meaningfully affect the TTR population in the cell (Fig. 3*B*). Hspa13 overexpression, on the other hand, nearly halves the relative mature fraction; MG132 treatment still has no further effect. Over the course of the chase, Hspa13 levels remain unchanged, suggesting a stable population. Mature ^{Flag}TTR rapidly decreases in the presence or the absence of Hspa13 (Figs. 3*B* and S3), consistent with its known secretion with a 3 h half-life (41, 71). The immature fraction, however, does not change over this time frame, neither in the presence nor in the absence of MG132, indicating that its degradation is slow. After 4 h, the relative amount of mature and immature TTR plateaus to the same ratio under all conditions (Fig. 3*C*). Hence, we can conclude that Hspa13-dependent mistargeted TTR accumulates and is persistent, with proteasomal degradation only becoming significant on the time scale of days (Fig. 1*C*). This relative resistance to proteasomal degradation could be due to the high thermodynamic and kinetic stability of TTR (40, 41) or to its propensity for aggregation if unable to fold (72).

Mislocalized ^{Flag}TTR forms insoluble aggregates

The accumulation of mislocalized protein presents a challenge for cytosolic protein homeostasis, as secretory proteins are prone to misfold and aggregate in the absence of proper maturation (3, 73). We hypothesized that accumulation of immature ^{Flag}TTR in the cytosol following Hspa13 overexpression could lead to TTR aggregation. The thermodynamic stability of TTR amyloid aggregates makes them relatively resistant to denaturation, even when boiled in Laemmli buffer prior to SDS-PAGE gels (74, 75). Even native TTR tetramers tend to preserve some dimer structure under these conditions. To look for stable TTR aggregates, we co-overexpressed ^{Flag}TTR and Hspa13 in HEK293T cells, limited boiling of lysates in reducing Laemmli buffer (including 2% SDS) to only 5 min, and separated lysates using gradient acrylamide SDS-PAGE gels that cannot effectively separate TTR isoforms but allow us to probe higher molecular weight ranges (Fig. 4, *A* and *B*). Expression of ^{Flag}TTR alone leads to a prominent dimer band, but about half of the TTR is present in the monomer range. By contrast, Hspa13 overexpression leads to over 80% of TTR presenting as high molecular weight. Similar results were also obtained in SH-SY5Y cells (Fig. S4*A*). Consistent with aggregates, long boiling times in Laemmli buffer reduce the high–molecular weight fraction, with little aggregate remaining after 30 min (Fig. S4*B*). An alternative explanation for high molecule weight TTR immunoreactivity could be TTR ubiquitination. To test this hypothesis, we overexpressed C-terminally hemagglutinin (HA)-tagged ubiquitin (Ub^{HA}) (76) alongside ^{Flag}TTR and Hspa13 and lysed in the presence of 12.5 mM *N*-ethylmaleimide to inactivate cellular deubiquitinases. The highly destabilized TTR^{D18G}, a canonical ERAD substrate (77), was transfected as a positive control for a known ubiquitinated protein (78). As expected, anti-Flag immunoprecipitation of $^{Flag}TTR^{D18G}$ provides a robust ubiquitination signature that is entirely dependent on proteasomal inhibition with MG132 (Fig. S4*C*). The WT ^{Flag}TTR, unexpectedly, shows noticeable ubiquitination even in the absence of MG132. This could be related to the slow clearance of mislocalized TTR (Fig. 3). Nevertheless, Hspa13 does not affect the ubiquitination of TTR, demonstrating that high molecular weight TTR under conditions of Hspa13 co-overexpression is not because of increased ubiquitination.

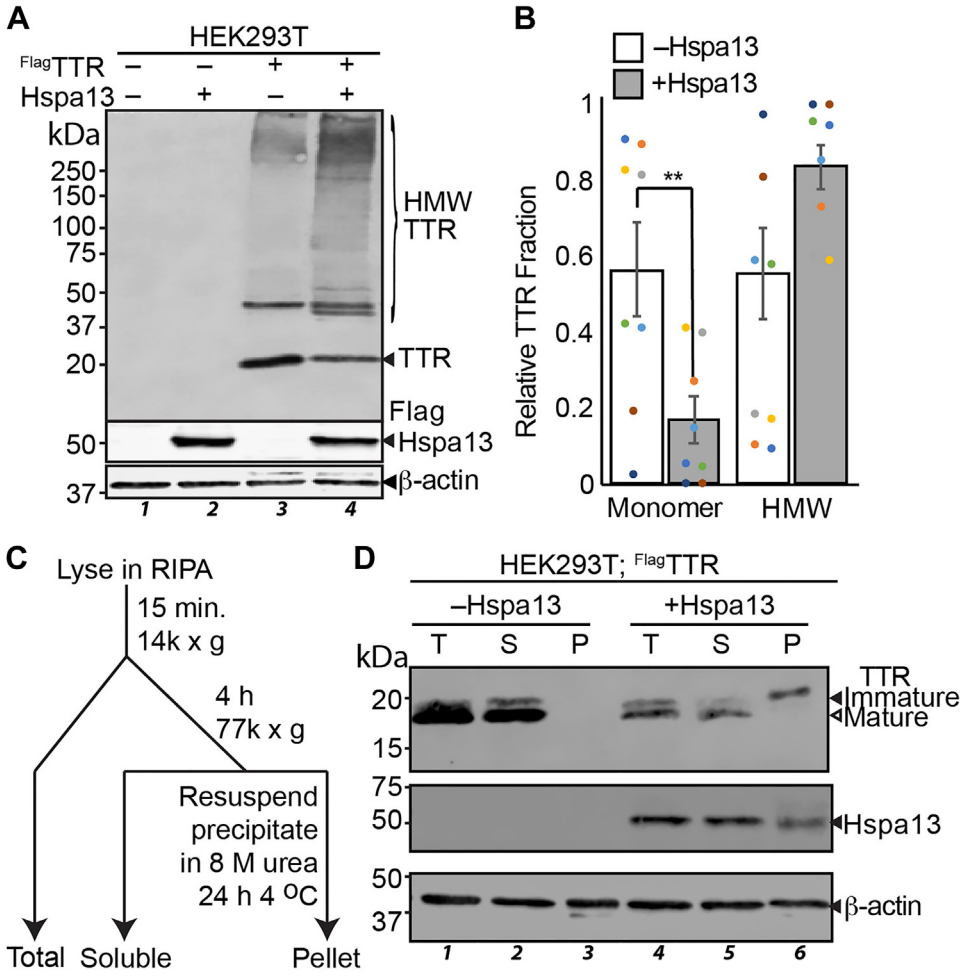

Figure 4. Mislocalized ^{Flag}TTR forms insoluble aggregates. *A*, representative immunoblot of lysates from HEK293T cells co-overexpressing ^{Flag}TTR and Hspa13 as indicated. Lysates were boiled for 5 min in Laemmli prior to separation by 4% to 20% gradient reducing SDS-PAGE. HMW indicated high molecular weight, as opposed to monomeric, TTR species. *B*, densitometric quantification of monomeric and HMW TTR fractions (n = 8). Error represents standard error of the mean. $^{**}p < 0.01$ by paired two-tailed Student's *t* test. *C*, schematic describing ultracentrifugation to separate protein aggregates. *D*, representative immunoblot of SDS-PAGE separated lysates from HEK293T cells overexpressing ^{Flag}TTR and Hspa13 as indicated. Lysates were fractionated as described in *C*. "T" indicates total lysate before centrifugation; "S" indicates soluble fraction; and "P" indicates the pellet. Equal percentages of prespin lysate were added to enable mass balance. ^{Flag}TTR, Flag-tagged TTR; HEK293T, human embryonic kidney 239T cell line; TTR, transthyretin.

To further probe changes in TTR solubility with Hspa13 overexpression, we used ultracentrifugation to separate insoluble aggregates from cellular lysates (Fig. 4*C*). After clearing chromosomal fractions and cellular debris from protein lysates with a 14,000*g* spin for 15 min, lysates were quantified, normalized for protein content, and then subjected to ultracentrifugation at 77,000*g* for 4 h at 4 °C. The resulting pellets were washed with RIPA buffer, and then solubilized by incubating in 8 M urea for 24 h at 4 °C. In the absence of Hspa13 overexpression, ^{Flag}TTR is completely soluble under these conditions (Fig. 4*D*). Hspa13 overexpression induces a population of insoluble ^{Flag}TTR, and the migration of this population is consistent with it being immature. These results support a model wherein Hspa13 overexpression inhibits ^{Flag}TTR import, leading to the accumulation of immature aggregation-prone TTR in the cytosol. We also compared the effect of Hspa13 overexpression to UPR induction by thapsigargin (Tg), which promotes secretion of aggregation-prone conformations of TTR (79). While Tg upregulates the UPR target BiP, and modestly inhibits TTR import efficiency (44, 46), it does not increase insoluble TTR to a similar extent as Hspa13 overexpression does (Fig. S4*D*). The aggregation propensity of cytosolic TTR likely explains why some of the immature TTR is insoluble under low-detergent conditions (Fig. S1*D*).

We considered that Hspa13 might have a similar effect on endogenous HEK293T proteins. To discover such proteins, we transfected HEK293T cells with either Hspa13 or mock (eGFP in the same plasmid vector). Total and insoluble lysates were prepared according to the same scheme of Figure 4*C*, and triplicates were prepared for multiplexed quantitative proteomics with a single run for the six total lysate samples, and a single run for the six pelleted samples (Fig. S4*E*). After filtering likely contaminants, we quantified 3372 proteins in the lysates and 1471 proteins in the pellets. We see no meaningful and significant difference in the cellular proteomes for cells overexpressing Hspa13 as compared with those expressing eGFP (Fig. S4*F* and Table S2), with the exception of Hspa13 and GFP

themselves. Crnkl1 (fold change [FC] = 0.62 ± 0.21, p [moderated] = 8.7×10^{-5}, q_{BH} = 0.098) and Dimt1 (FC = 0.23 ± 0.08, p [moderated] = 7.6×10^{-4}, qBH = 0.43) are possibly differential but do not pass our threshold of $q_{BH} < 0.05$. Similarly, in the pelleted insoluble fraction (Fig. S4*G* and Table S3), only Hspa13 and GFP pass our significance threshold, though Fasn (FC = 1.17 ± 0.04, p [moderated] = 5.2×10^{-4}, q_{BH} = 0.26) and Myh10 (FC = 1.36 ± 0.16, p [moderated] = 3.7×10^{-3}, q_{BH} = 0.44) are potentially differential. Hence, under basal conditions, Hspa13 overexpression remodels neither the proteome nor its solubility.

Hspa13 ATPase mutants exacerbate TTR import deficits and aggregation

Similar to other Hsp70 proteins, Hspa13 contains an NBD and is an active ATPase (29). In most Hsp70s, ATP hydrolysis is stimulated by client and Hsp40 binding, leading to a conformational change in the SBD that increases affinity for and unfolding of the client protein (27). ATPase activity can also be increased with peptide sequences that mimic full-length clients (80). Unlike other Hsp70s, Hspa13 ATPase activity is not stimulated by peptide binding, consistent with its lack of an SBD (29). In the absence of a clear function for Hspa13 ATPase activity, we considered that this activity might influence its effect on ER import. We prepared two Hspa13 constructs that we expected to be ATPase deficient, based on the high conservation of this domain between Hspa13 and other Hsp70s, and the well-characterized nature of these mutations across multiple Hsp70 proteins (Fig. 5*A*). Briefly, BiP T229G and DnaK T199A do not affect ATP binding but decrease ATP hydrolysis by ≥95% (81, 82). Similarly, DnaK K70A and Hsc70 K71A bind ATP but cannot hydrolyze it (83, 84). We assessed $Hspa13^{K100A}$ and $Hspa13^{T230A}$ for their induction of immature and aggregated TTR using the ultracentrifugation assay (Fig. 5*B*). As with the WT Hspa13, overexpression of either ATPase-inactive $Hspa13^{K100A}$ or $Hspa13^{T230A}$ increases the amount of immature and insoluble TTR. This effect is greater for $Hspa13^{K100A}$ than for WT, and $Hspa13^{T230A}$ expression partitions almost all TTR to the immature and insoluble population. ^{Flag}TTR contains the Flag tag adjacent to the native TTR signal peptide cleavage site, which could affect behavior of the signal peptide. We hence also evaluated the effect of Hspa13 mutant coexpression with untagged TTR. Although $Hspa13^{K100A}$ and $Hspa13^{T230A}$ still inhibit TTR maturation and promote its aggregation, $Hspa13^{WT}$ does not have an effect on the untagged protein (Fig. S5), implying that the effect of Hspa13 on import is sensitive to signal peptide context. Although we cannot yet speculate as to the role of ATPase function regarding protein import into the ER, it is clear that the effect of Hspa13 overexpression is exacerbated by loss of ATPase function. Impaired translocon function could be deleterious to cellular fitness. To test this hypothesis, we overexpressed $Hspa13^{WT}$, $Hspa13^{T230A}$, or eGFP (mock) in the same plasmid vector in HEK293T cells.

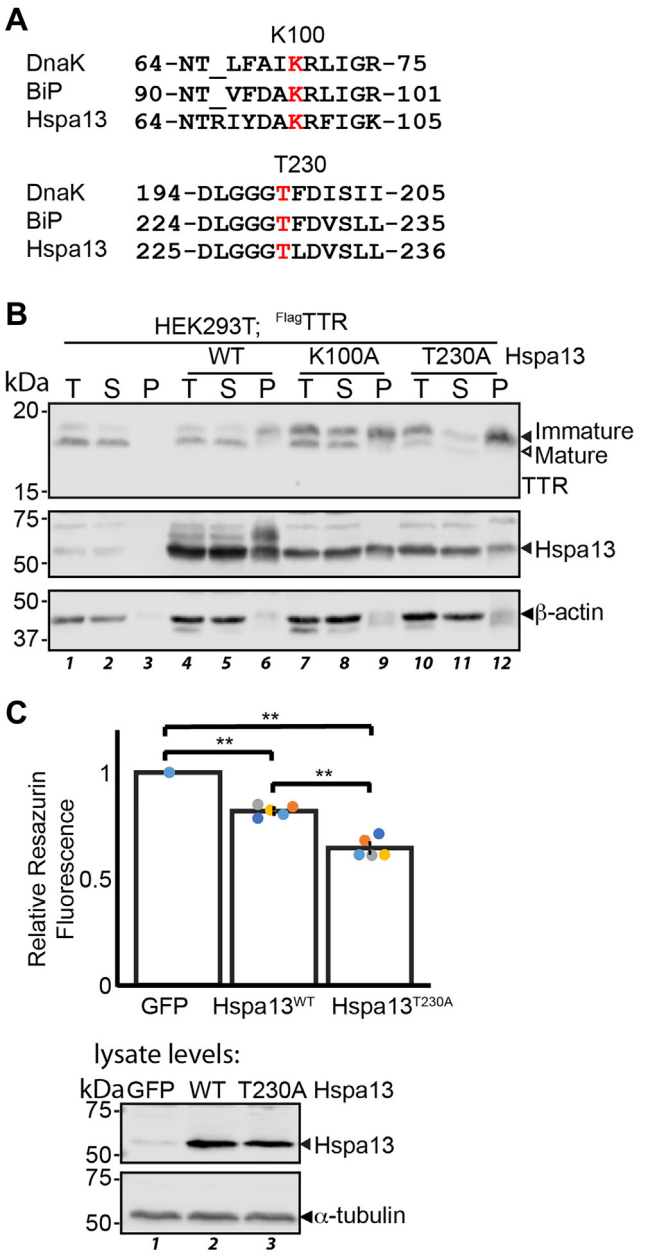

Figure 5. Hspa13 ATPase mutants exacerbate TTR import deficits and aggregation. *A*, schematic depicting conservation between DnaK, BiP, and Hspa13 in the vicinity of known DnaK/BiP ATPase mutants. The sites of mutation are indicated in *red*. *B*, representative immunoblot of SDS-PAGE separated lysates from HEK293T cells overexpressing ^{Flag}TTR and Hspa13 as indicated. Lysates were fractionated as described for Figure 4*C*. "T" indicates total; "S" indicates soluble fraction; and "P" indicates the pellet. *C*, normalized (to mock GFP overexpression) resazurin fluorescence (excitation: 560 nm; emission: 570 nm) from HEK293T cells overexpressing Hspa13 variants as indicated. Cells were seeded at 7500 cells/well, and wells were individually transfected the next day with 21 μl of DNA/$Ca_3(PO_4)_2$ for 16 h. Cells were incubated with fresh media containing resazurin (25 μg/ml) for 2 h prior to measurement. Significance was assessed by ANOVA ($n = 5$; $F = 182 > F_{crit} = 3.9$) followed by Tukey's post hoc HSD. $^{**}p < 1 \times 10^{-5}$. An immunoblot from cells transfected in parallel is shown below. BiP, binding immunoglobulin protein; ^{Flag}TTR, Flag-tagged TTR; HEK293T, human embryonic kidney 239T cell line; HSD, honestly significant difference; TTR, transthyretin.

Cellular proliferation was determined by the resazurin metabolic assay. Indeed, $Hspa13^{WT}$ and $Hspa13^{T230A}$ overexpression decrease cellular viability by 18% ± 1% and 36% ± 2%, respectively (Fig. 5*C*).

Hspa13 overexpression and mutation impair secretory proteostasis

Translocation kinetics are closely tied to processing and maturation in the ER. Signal peptide cleavage frees the C terminus of luminal proteins for cotranslational processing and folding (85). Poorly optimized signal sequences demonstrate decreased glycan occupancy (86, 87). If Hspa13 modulation disrupts translocon function, that could also affect proteostasis of secretory proteins that still successfully enter the ER. Consistent with this hypothesis, Hspa13 co-overexpression inhibits NKCC2 glycan maturation in HEK293 cells (36). To evaluate proteostasis of mature TTR, we exploited the well-characterized affinity of ER chaperones for destabilized TTR (78, 88, 89). ^{Flag}TTR was co-overexpressed with either Hspa13 or the other ER Hsp70, BiP. A C-terminal myc tag on BiP allows us to differentiate between the transfected and endogenous protein. ^{Flag}TTR^{D18G}, a highly destabilized variant of TTR, was also transfected as a positive control, and each sample immunoprecipitated to see TTR-associated chaperones. As previously reported, TTR^{D18G} robustly immunopurifies with both BiP and the ER Hsp40 ERdj3 (Fig. 6*A*). ^{Flag}TTR^{WT}, which is both kinetically and thermodynamically stable, does not associate with either chaperone. BiP overexpression is sufficient to induce some BiP

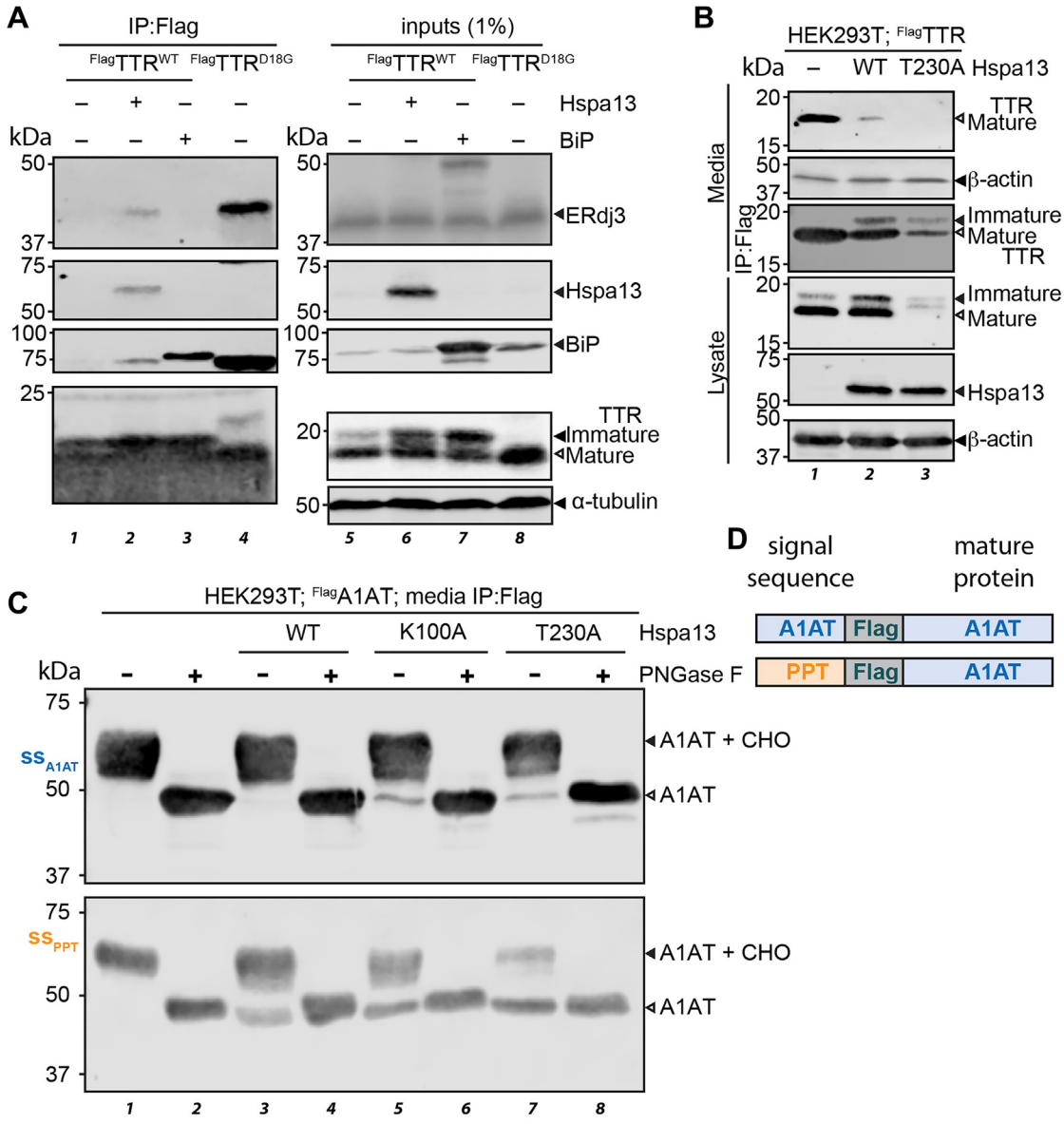

Figure 6. Hspa13 overexpression and mutation impair secretory proteostasis. *A*, representative immunoblots of SDS-PAGE separated lysates and M2 anti-Flag immunoisolates from HEK293T cells overexpressing ^{Flag}TTR variants, Hspa13, and hamster BiP^{myc} as indicated. *B*, representative immunoblots of SDS-PAGE separated lysates, conditioned media, and conditioned media M2 anti-Flag immunoisolates from HEK293T cells overexpressing ^{Flag}TTR and Hspa13 variants as indicated. Media were conditioned for 29 h. Quantification in Fig. S6*B*. *C*, representative immunoblots of SDS-PAGE separated M2 anti-Flag immunoisolates from HEK293T cells overexpressing ss$_{A1AT}$^{Flag}A1AT or ss$_{PPT}$^{Flag}A1AT and Hspa13 variants as indicated. Media were conditioned for 24 h prior to IP. *D*, schematic illustrating the two A1AT constructs employed. A1AT, alpha-1 antitrypsin; BiP, binding immunoglobulin protein; ^{Flag}TTR, Flag-tagged TTR; HEK293T, human embryonic kidney 239T cell line; IP, immunoprecipitation.

copurification with TTR^{WT} but does not induce ERdj3 association. This suggests that while BiP overexpression can drive BiP association to TTR^{WT}, it does not induce destabilization of the protein. Hspa13 overexpression, however, induces binding of both BiP and ERdj3 to TTR^{WT}, indicating a destabilized population of TTR in the ER. This suggests that ER proteostasis is impaired by Hspa13 overexpression. It is worth noting that BiP overexpression also leads to an increase in immature TTR (Fig. 6*A*, lanes 3 and 7), and this immature population is localized to the cytosol (Fig. S6*A*). However, this effect is not simply because of overexpression of abundant ER chaperones, as overexpression of ERdj3 does not affect TTR maturation and localization (Fig. S6*A*). Similarly, HYOU1 overexpression only slightly affects TTR localization (Fig. S6*A*), consistent with UPR activation by HYOU1 and consequent BiP overexpression (Fig. S1*E*). A more detailed investigation of BiP overexpression and TTR translocation will be addressed in a separate article.

Since TTR ER proteostasis is inhibited by Hspa13 overexpression, we considered the effect of Hspa13 overexpression on secretion. HEK293T cells were transfected with ^{Flag}TTR and either $Hspa13^{WT}$ or $Hspa13^{T230A}$, the media changed after 16 h, and then media conditioned for another 24 h. Overexpression of $Hspa13^{WT}$ nearly eliminates ^{Flag}TTR secretion, despite a substantial mature population persisting in the cells (Figs. 6*B* and S6*B*). Following $Hspa13^{T230A}$ co-overexpression, almost no ^{Flag}TTR secretion is observed. To better determine the relative amounts of secreted ^{Flag}TTR for Hspa13 variant co-overexpression, we immunoprecipitated ^{Flag}TTR from the media using anti-Flag antibody. Immunoprecipitation allows the small amount of residual TTR secreted from $Hspa13^{T230A}$ cells to be visualized. It also reveals that there is a small population of immature TTR secreted with Hspa13 overexpression. We do not see significant change in β-actin accumulation in the conditioned media, indicating that there is no substantial cell lysis; however, the faint amount of immature TTR with Hspa13 cotransfection could be due to a small number of lysed cells. Brefeldin A is a small molecule that rapidly collapses the Golgi and is often used to decipher whether a protein is secreted through the canonical secretory pathway (90–92). Brefeldin A treatment abolishes secretion of the mature TTR population but does not decrease the immature population. This indicates that while the mature TTR is trafficked through the secretory pathway, the immature portion is bypassing the Golgi through another mechanism, such as necrosis (Fig. S6*C*). To determine the generality of this phenotype, we also considered the effect of Hspa13 on TTR secretion from another cell line. Chinese hamster ovary (CHO)-K1 cells were cotransfected with $^{Flag}TTR^{WT}$ and either GFP (mock), $Hspa13^{WT}$, or $Hspa13^{T230A}$. Similarly to the case with HEK239T cells, $Hspa13^{WT}$ overexpression increases the amount of immature TTR and detergent-resistant high–molecular weight species (Fig. S6*D*). The immature to mature ratio of TTR increases more with $Hspa13^{T230A}$ expression. $Hspa13^{WT}$ overexpression decreases TTR secretion by about 20%, whereas $Hspa13^{T230A}$ decreases TTR secretion by about 65% (Fig. S6*E*).

We further considered another secretory protein, alpha-1 antitrypsin (A1AT). A1AT is a metastable N-glycosylated hepatically secreted protein (93, 94). Destabilizing mutations in A1AT lead to its aggregation or degradation in the cell, suppressing secretion and ultimately leading to diseases associated with A1AT serum deficiency and/or hepatic aggregation (95). We co-overexpressed Hspa13 variants with an A1AT construct with Flag situated C-terminal to the endogenous signal peptide. Hspa13 overexpression neither inhibits A1AT import into the ER nor does it noticeably affect its secretion (Fig. S6, *F–H*). $Hspa13^{T230A}$ overexpression, on the other hand, substantially decreases A1AT levels in the cell and its secretion. We also observed a small amount of non-glycosylated secreted A1AT with overexpression of both Hspa13 ATPase mutants (Fig. S6*G*). The identity of the band was confirmed by treatment with PNGase F, which removes N-linked glycans and resolves both bands together (Fig. 6*C*). Because glycan occupancy is linked to signal sequence identity, and weaker signal sequences show greater reliance on translocon-associated complexes such as TRAP and Sec62/63 (15, 96), we considered whether Hspa13 overexpression would have a larger effect on a protein harboring a weaker signal sequence. We replaced the signal sequence on ^{Flag}A1AT with that of preprotrypsin (Fig. 6*D*), which has a far shorter hydrophobic region; hydrophobicity is necessary to engage both SRP and Sec61 (97, 98). The A1AT *N*-glycosylation sequons, N70, N107, and N271, are far from the N terminus (99, 100). As is the case for $ss_{A1AT}{}^{Flag}$A1AT, $ss_{ppt}{}^{Flag}$A1AT is secreted solely as the mature glycosylated form (Fig. 6*C*). However, the sensitivity to Hspa13 is now much greater, with $Hspa13^{WT}$ overexpression now inducing noticeable secretion of immature and nonglycosylated ^{Flag}A1AT, whereas $Hspa13^{T230A}$ expression now leads to secretion of almost solely the non-glycosylated form. Hence, it is clear that in addition to its effects on ER translocation and cytosolic proteostasis, Hspa13 expression affects protein maturation in the ER.

Hspa13 knockout impairs TTR proteostasis in the ER

Having established that Hspa13 overexpression and mutation inhibit translocation, we looked to see the effect of ablating Hspa13. We generated $HSPA13^{-/-}$ cells using the *Streptomyces pyogenes* CRISPR/Cas9 system (Figs. 7*A* and S7*A*) (101). Single clones were assessed for Hspa13 expression, and two $HSPA13^{-/-}$ lines were chosen for expansion: 1A3 and 12F4. While 12F4 grows normally and has similar BiP expression to HEK293T cells, 1A3 grows slowly and has highly upregulated BiP expression, suggesting constitutive UPR activation (Figs. 7*B* and S7*B*). In the 12F4 line, TTR maturation appears unaffected as compared with the parental line (Fig. 7*B*). However, upon treatment with the canonical UPR chemical inducer Tg, we observe a few differences between the $HSPA13^{-/-}$ and the parental line. First, Tg induces high–molecular weight and insoluble TTR aggregates in 12F4 $HSPA13^{-/-}$ cells (Fig. 7, *B* and *C*). Second, while Tg induces immature TTR in both cell lines, presumably through the preemptive quality control pathway (44, 45), the effect is

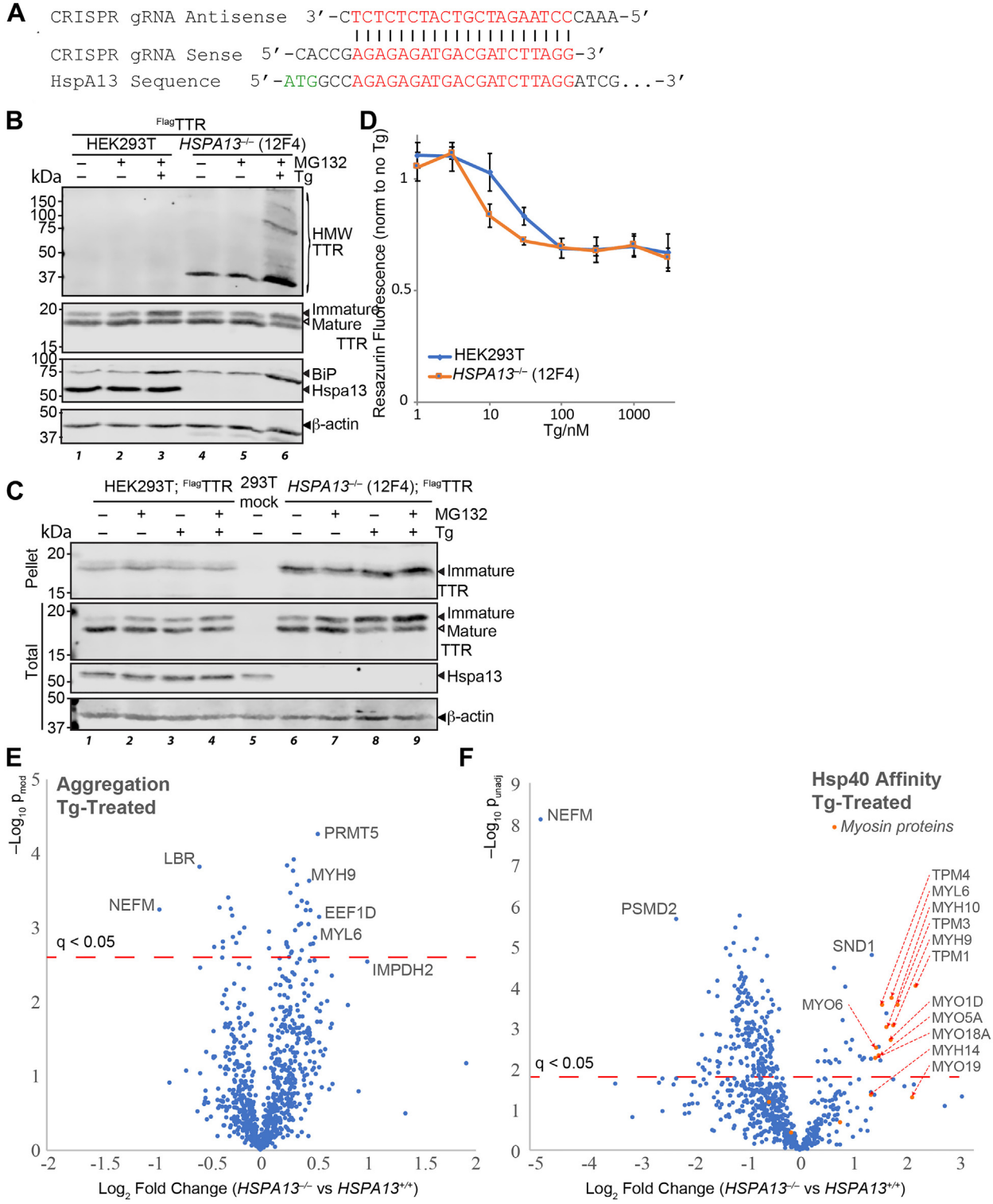

Figure 7. Hspa13 knockout impairs TTR proteostasis in the ER. *A*, schematic of guide RNA sequences used to direct Cas9 cleavage to *HSPA13*. *B*, representative immunoblot of SDS-PAGE separated lysates from HEK293T or *HSPA13*$^{-/-}$ (12F4) cells overexpressing ^{Flag}TTR and treated with MG132 (100 nM; 16 h) and/or Tg (10 nM; 16 h) as indicated. HMW TTR is resolved on 4 to 20% gradient gels following 5 min boiling in reducing Laemmli buffer, whereas immature and mature TTR monomers are resolved using 15% gels after 20 min boiling. *C*, representative immunoblot of SDS-PAGE separated lysates from HEK293T or *HSPA13*$^{-/-}$ (12F4) cells overexpressing ^{Flag}TTR and treated with MG132 (200 nM; 16 h) and/or Tg (50 nM; 16 h) as indicated. Lysates were fractionated as described for Figure 4*C*. *D*, normalized resazurin fluorescence (excitation: 560 nm; emission: 590 nm) signal of HEK293T or *HSPA13*$^{-/-}$ (12F4) cells incubated with Tg (16 h) as indicated. Cells were seeded at 15,000 cells per well 2 h prior to Tg treatment (16 h). Media containing resazurin (25 μg/ml) were added to cells 2 h prior to measurement (n = 3). *E*, volcano plot for the relative recovery of aggregated proteins from *HSPA13*$^{-/-}$ knockout (12F4) cells as opposed to the parental *HSPA13*$^{+/+}$ HEK293T line. The *red dashed line* indicates the false discovery rate threshold of 5%, as determined by the Benjamini–Hochberg method. *F*, volcano plot for the relative recovery of destabilized protein, as determined by Hsp40 affinity, from *HSPA13*$^{-/-}$ knockout (12F4) cells as opposed to the parental *HSPA13*$^{+/+}$ HEK293T line. The *red dashed line* indicates the false discovery rate threshold of 5%, as determined by the Benjamini–Hochberg method. ^{Flag}TTR, Flag-tagged TTR; HEK293T, human embryonic kidney 239T cell line; HMW, high molecular weight; Tg, thapsigargin; TTR, transthyretin.

exacerbated in the 12F4 *HSPA13*$^{-/-}$ cells. Finally, the sensitivity to Tg is greater in 12F4 *HSPA13*$^{-/-}$ cells as determined by the resazurin metabolic activity assay (Fig. 7*D*). The 1A3 *HSPA13*$^{-/-}$ cell line, by contrast, is resistant to Tg toxicity (Fig. S7*C*), consistent with its UPR activation. Hormetic UPR activation has been shown to both enhance TTR quality control and to protect against Tg toxicity (71, 78, 79, 102).

We further explored how *HSPA13* knockout could affect protein homeostasis during stress using two assays for protein stability. In the first approach, we treated *HSPA13*$^{+/+}$ and 12F4 *HSPA13*$^{-/-}$ cells with Tg (50 nM; 16 h), prior to subjecting them to ultracentrifugation as in Figure 4*C*. Pelleted protein was reduced, alkylated, digested to peptides, labeled with TMT tags, and analyzed by LC–MS/MS (n = 3). We found 42 proteins with significantly different levels in the pellet, with the largest changes for neurofilament medium chain (NEFM; FC = 0.52 ± 0.08, p = 6×10^{-4}, q = 0.03), elongation factor 1-delta (EEF1D; FC = 1.46 ± 0.16, p = 7×10^{-4}, q = 0.03), lamin B receptor (LBR; FC = 0.67 ± 0.05, p = 2×10^{-4}, q = 0.03), and the major nonmuscle myosin IIA components MYH9 (FC = 1.37 ± 0.09, p = 2×10^{-4}, q = 0.03) and MYL6 (FC = 1.42 ± 0.14, p = 1×10^{-3}, q = 0.044) (Figure 7*E*). The disease-associated aggregation-prone protein inosine 5′-monophosphate dehydrogenase 2 (IMPDH2; FC = 2.00 ± 0.57, p = 3×10^{-3}, q = 0.053) displays a notable change that did not reach the 0.05 FDR significance threshold. In the second approach, we used our recently reported assay for protein destabilization, in which affinity to the Hsp40 DNAJB8^{H31Q} is used as a proxy for stability (103). We overexpressed DNAJB8^{H31Q} in *HSPA13*$^{+/+}$ and 12F4 *HSPA13*$^{-/-}$ cells prior to treatment with Tg (1 μM, 3 h), followed by DNAJB8^{H31Q} immunoprecipitation and TMT-LC–MS (Figure 7*F*). We find a sharp decrease in the load of destabilized NEFM (FC = 0.03 ± 0.04, p = 8×10^{-9}, q = 6×10^{-6}) and increased destabilization across the myosin family, including MYH9 (FC = 3.7 ± 2.3, p = 9×10^{-4}, q = 0.008) and MYL6 (FC = 3.3 ± 2.1, p = 2×10^{-4}, q = 0.004). It is possible that the decreased load of destabilized and aggregated NEFM is a reflection of the increased destabilization of myosin, as myosins are involved in the transport and positioning of neurofilaments (104).

Discussion

ER delivery of soluble secretory proteins is canonically encoded by the signal peptide. However, differences in signal peptide chemistry and cellular stress can influence both the targeting of proteins to the ER as well as the maturation of proteins in the ER. Mislocalization and differential maturation in turn can affect both cytosolic and secretory proteostasis (4, 105–107). To understand the substrate-specific stringency of the translocon, as well as how stress can modulate this stringency, we need to determine the cellular components that modulate translocational activity. Herein, we have demonstrated that Hspa13 function impacts the stringency of translocational substrate import and maturation of two model secretory proteins: TTR and A1AT. Hspa13 specifically binds a majority of translocon subunits as well as members of complexes associated with cotranslocational glycosylation and signal peptide cleavage. This is in sharp contrast to the other ER Hsp70, BiP, which has a wide-ranging interaction network that does not particularly feature translocon components (108, 109). In combination with previous reports of Hspa13 expression levels sensitizing mice to prion toxicity (21, 110), and to the synthetic toxicity of signal peptidase inhibition with *HSPA13* knockout (20), the present work further points to a role of Hspa13 in regulating the import and processing of nascent secretory proteins.

While these studies demonstrate that Hspa13 can interfere with secretory protein import and processing, they do not demonstrate that Hspa13 acts in such a manner in a particular disease state. TTR neither is natively expressed in HEK293T cells nor does it harbor a Flag tag after its signal sequence. Indeed, we see that TTR without the Flag tag is less prone to mislocalization, and the Hspa13 overexpression effect is ablated. Even in this case, the ATPase mutants promote mistargeting. Similarly, glycosylation of A1AT with its native signal sequence is unaffected by Hspa13^{WT} overexpression but is inhibited by overexpression of either of the Hspa13 ATPase mutants. Generally, every effect that we observe as a consequence of Hspa13^{WT} overexpression is greater for Hspa13^{K100A} and even greater for Hspa13^{T230A}. Why would loss of ATPase activity exacerbate an effect associated with overexpression? The answer could be related to the function of the NBD in full-length Hsp70s (111). The SBDs in these proteins consist of two domains, SBDα and SBDβ. The ATP-bound form of Hsp70 forms rigid interactions between NBD and SBDβ. This interaction inhibits ATP hydrolysis, while also preventing tight binding to substrate through SBDα–SBDβ clamping. Hsp40 J-domain and substrate binding both serve to modulate this interaction, allowing the NBD to more readily access a conformation that is competent to hydrolyze ATP, thus releasing SBDβ. Hspa13 lacks the SBD but does contain most NBD sites that interact with the Hsp40 J-domain. If this surface dysregulates import phenotypes through a direct binding event, then Hspa13 overexpression would increase the available Hspa13 for binding. In turn, ATPase mutants would maintain this surface in a higher-binding affinity conformation. We do see Hspa13 interactions with two translocon-associated Hsp40 proteins associated with post-translational ER import through Sec61: Sec62 and Sec63 (14). Hspa13 might interact with these proteins to affect their function or indirectly compete with their association with BiP. Consistent with this possibility, A1AT with a weaker signal sequence was more sensitive to Hspa13 overexpression. Weaker signal sequences increase the reliance on post-translational translocation (15, 112). Further investigations will need to establish the molecular mechanism by which Hspa13 regulates import as well as how this depends on the many other chaperones and stress factors that bind to and regulate the translocon (14, 113, 114), yielding a polydisperse distribution of translocon compositions (115, 116) that impact import and maturation (117).

Pre-emptive quality control is one of the least characterized consequences of UPR activation. Given that Hspa13 is a UPR-responsive target, and that it leads to TTR import inhibition,

one might speculate that Hspa13 upregulation mediates preemptive quality control by the UPR. However, preemptive quality control is not interrupted in either of the *HSPA13*$^{-/-}$ cell lines, establishing that Hspa13 does not mediate this process. Rather, Hspa13 knockout aggravates the maturation (and presumably import) inhibition induced by Tg in the 12F4 line. In the 1A3 clonal *HSPA13*$^{-/-}$ line, where constitutive UPR activation offers hormetic protection, Tg interferes with TTR maturation to a similar extent as the parental HEK293T line. In the absence of stress, *HSPA13* knockout also does not affect TTR maturation. Nevertheless, TTR aggregation is greater in the *HSPA13* knockout line, demonstrating impaired ER proteostasis. Similarly, Hspa13 overexpression leads to increased association between mature TTR and ER chaperones. It is clear that modulating Hspa13 levels in either direction is deleterious for the ER.

Experimental procedures

Plasmids

Expression constructs for Hspa13 and its variants were prepared in the pDEST30 vector. Hspa13 was amplified from HEK293T-derived complementary DNA (cDNA) and ligated into the pENTR1A vector using SalI and EcoRV restriction sites. HYOU1 was amplified from HEK293T-derived cDNA and ligated into the pENTR1A vector using SalI and EcoRI restriction sites. The genes were then transferred into the pDEST30 vector by homologous recombination using the Gateway kit (Thermo). Hspa13 variants were prepared by site-directed mutagenesis. Hspa13^{Flag} was prepared from the Hspa13.pDEST30 plasmid by PIPES cloning (118). ERdj3 and BiP plasmids have been reported (88). ^{Flag}TTR and ^{Flag}TTR^{D18G} in the pcDNA3.1 vector have been reported (71). Ubiquitin^{HA} in the pcDNA backbone was a gift from Edward Yeh (Addgene plasmid #18712; http://n2t.net/addgene:18712; Research Resource Identifier [RRID]: Addgene_18712) (76). ^{cyt}APEX2 in the pcDNA3 backbone was a gift from Alice Ting (Addgene plasmid #49386; http://n2t.net/addgene:49386; RRID: Addgene_49386) (51). pCMV-^{ER}HRP^{N175S} was a gift from Joshua Sanes (Addgene plasmid #79909; http://n2t.net/addgene:79909; RRID: Addgene_79909) (50). CRISPR vector pX330A-1x2 was a gift from Takashi Yamamoto (Addgene plasmid #58766; http://n2t.net/addgene:58766; RRID: Addgene_58766) (101). Targeting primers were ligated into BbsI-cleaved pX330A-1x2 to generate the *HSPA13*-targeting plasmid. Primers for all cloning procedures described are listed in Table S4.

Mammalian cell culture

HEK293T cells and derived lines were grown in Dulbecco's modified Eagle's medium (DMEM) (Corning) with 10% fetal bovine serum (Seradigm), penicillin–streptomycin antibiotic cocktail, and L-glutamine. SH-SY5Y and CHO-K1 cells were similarly grown in DMEM/Ham's F-12 with the same supplements. Calcium phosphate transfection for HEK293T and SH-SY5Y cells was performed as previously reported (54) with media change within 16 h of transfection. CHO-K1 cells were transfected by the polyethyleneimine method. Unless otherwise indicated, cells were harvested by rinsing in 1× PBS (HyClone), scraping from the plates, and lysis in RIPA buffer (50 mM Tris [pH 7.4], 150 mM NaCl, 1% Triton X-100, 0.5% sodium deoxycholate, and 0.1% SDS) containing cOmplete protease inhibitor (Roche Diagnostics). Cells expressing Ub^{HA} were lysed in the presence of 12.5 mM *N*-ethyl maleimide. Lysis involved resuspension of cells and incubation on ice for 15 min, followed by a full-speed hard spin at 4 °C for 20 min. Media conditioning was performed for 24 h, starting 12 to 16 h post-transfection, unless otherwise indicated. Conditioned media were collected and spun at 700*g* for 5 min to remove cellular debris. For Flag enrichments, M2-anti-Flag dynabeads (Sigma) were incubated with cultured media and rotated overnight at 4 °C. Protein was eluted by boiling in 4× Laemmli buffer, and then eluates were collected and reduced with 20 mM DTT and further boiling for 20 min.

Resazurin assays

Cells were incubated with DMEM containing resazurin (25 μg/ml; Acros Organics) for 2 h. Fluorescence from cells was measured *via* a Synergy H1 microplate reader set for 560 nm excitation and 590 nm emission.

Proximity labeling

We used ^{ER}HRP and ^{cyt}APEX2 labeling to biotinylate proteins that are targeted to the ER-luminal space and cytosol, respectively (46, 119, 120). Unless otherwise indicated, cells were treated with 1 μM MG132 treatment for 16 h prior to harvesting to inhibit proteasomal degradation. About 30 min prior to harvest, the media were changed to fresh complete media containing 500 μM biotin–phenol and 1 μM MG132. Immediately prior to harvesting, aqueous hydrogen peroxide (Fisher) was added to a final concentration of 1 mM, the plates were gently agitated, and incubated for exactly 1 min at ambient temperature. The reaction was quenched by washing three times with Dulbecco's PBS containing 5 mM Trolox, 10 mM sodium ascorbate, and 10 mM sodium azide. Cells were then lysed in RIPA buffer supplemented with protease inhibitor cocktail, 5 mM Trolox, 10 mM sodium ascorbate, and 10 mM sodium azide. Biotinylated protein was purified by incubation with avidin beads overnight with rotating at 4 °C. Beads were washed with the following buffers to remove nonspecific binders: twice with RIPA lysis buffer, once with 1.0 M KCl, once with 0.1 M Na_2CO_3, once with 2.0 M urea in 100 mM Tris, pH 8.0, and twice with RIPA lysis buffer. Biotinylated proteins were eluted by boiling the beads in elution buffer containing 12% SDS, 47% of glycerol in 60 mM Tris pH 6.8, with 10 mM DTT and 2 mM biotin for 10 min. The eluate was collected by centrifuging the beads and boiled for another 10 min.

Ultracentrifugation

Normalized cell lysates were spun in a Beckman Coulter Optima Max-XP for 4 h at 77,000*g*. The TLA-55 rotor was refrigerated at 4 °C and kept under vacuum during the

ultracentrifugation. Pellets were rinsed with RIPA and solubilized with 8 M urea over 4 days at 4 °C and then diluted with three parts of RIPA.

Immunoblotting

Samples were boiled in 16.7 mM DTT/Laemmli buffer for 20 min at 100 °C and resolved in homemade SDS-PAGE gels cast in Bio-Rad Mini-PROTEAN glass plate assemblies. Electrophoresis began at 65 V to allow sample stacking in the 4% acrylamide stacking gel, followed by 175 V for resolution in the resolving gel. A gel gradient from 4 to 20% was used for resolving high–molecular weight ^{Flag}TTR smears, whereas 12% or 15% was used for resolving ^{Flag}TTR monomers. Gradient gels were prepared by aspirating 4% activated gel solution into a pipette, an equal volume of 20% solution below it, and then aspirating three bubbles to generate the gradient, followed by careful dispensing into the gel cassette for polymerization. Protein was transferred to nitrocellulose membrane *via* semidry method (Bio-Rad *Trans*-Blot Turbo) for 1 h, using Towbin's buffer as a saturant for the filter paper padding. Blotted membranes were assessed for quality with Ponceau stain and then blocked with 5% milk in Tris-buffered saline (TBS) for 40 min at ambient temperature. The blots were serially rinsed with TBS with 1:1000 Tween-20 for 5 min per rinse and then incubated with primary antibody solution (primary antibody diluted in 5% bovine serum albumin, 0.1% sodium azide, and TBS) for 2 h. The blots were serially rinsed and incubated with secondary antibody solution (1:20,000 Li-COR near-IR fluorophore-conjugated secondary antibody diluted in 5% milk, TBS) for 20 to 40 min and imaged on a Li-COR Odyssey Fc.

PNGase F treatment

Lysates (20 μg) and media immunoprecipitates were diluted to 10 μl in 2× glycoprotein denaturing buffer (NEB) and boiled for 10 min at 100 °C. About 2 μl GlycoBuffer 2 10× (NEB), 2 μl NP-40, 1 μl PNGase F (NEB), and 5 μl water were added, and the solution was incubated at 37 °C for 1 h.

Knockout cell preparation

Knockout lines were prepared by transient transfection of HEK293T cells with pX330A-1x2 plasmid harboring the chosen guide RNAi, and transfected cells selected with zeocin. After selection, individual cells were monoclonally expanded, and Hspa13 protein expression was characterized to identify *HSPA13*$^{+/+}$, *HSPA13*$^{-/+}$, and *HSPA13*$^{-/-}$ lines.

Hsp40 affinity profiling

Six 10 cm dishes each of HEK293T and *HSPA13*$^{-/-}$ cells were transfected with ^{Flag}DNAJB8^{H31Q}, and 2 days later, these were treated with 1 μM Tg for 3 h. Cells were lysed as described previously with RIPA buffer containing protease inhibitors. Lysates were normalized by total protein content using Bradford Assay (Bio-Rad) and immunoprecipitated overnight at 4 °C over M2 anti-Flag Dynabeads (Sigma). The beads were washed four times with RIPA buffer, and Hsp40-associated proteins were eluted by boiling in Laemmli 6× buffer.

Sample preparation for MS

Protein samples were cleaned by methanol–chloroform precipitation. Dried protein pellets were reconstituted in 1% RapiGest (Waters or AOBIOUS) in 100 mM Hepes (pH 8.0). Disulfide bonds were reduced in 10 mM Tris(2-carboxyethyl) phosphine for 30 min in the dark and alkylated with 5 mM iodoacetamide for 15 min in the dark at room temperature. Proteins were then digested with trypsin at 1% (w/w) trypsin at 37 °C overnight. For each analysis, a triplicate of GFP control and a triplicate of Hspa13 overexpression were labeled with 6-plex TMT reagents (Thermo). Reagents were dissolved in acetonitrile and added to peptides (1:1) dissolved in 100 mM Hepes (pH 8.0) to a final acetonitrile concentration of 40% (v/v). The reactions were incubated for 1 h at room temperature and then quenched with ammonium bicarbonate at a final concentration of 0.4%. The samples were combined and evaporated to 10 μl and then brought to 200 μl by solvent A (5% acetonitrile and 0.1% formic acid). The pooled sample was acidified with 5% formic acid to pH 2. Samples were incubated at 37 °C and centrifuged at 21,100*g* for a few cycles to remove RapiGest.

LC–MS analysis

LC–MS experiments were performed on a Thermo LTQ Velos Pro equipped with an EASY-nLC 1000 nanoLC (Thermo). Buffer A is 5% aqueous acetonitrile and 0.1% formic acid. Buffer B is 80% aqueous acetonitrile and 0.1% formic acid. Peptides were initially loaded on a triphasic MudPIT trapping column and washed with buffer A. The columns were prepared from 100 μm ID fused silica (Molex) with a KASIL frit and loaded with 2.5 cm each of 5 μm Aqua C18 resin, Jupiter SCX resin, and 5 μm Aqua C18 resin (Phenomenex). After washing with buffer A and bumping from the first C18 phase to the SCX phase with an organic gradient, peptides were iteratively transferred to the second C18 phase with increasing injections of ammonium acetate (121). After each injection, the MuDPIT column was washed with buffer A, and then the peptides were separated over a 25 cm analytical column (100 μm ID, 5 μm tip pulled on a Sutter Instruments T-2000 tip puller) packed with 3 μm C18 resin (Phenomenex) using a gradient from 7% to 55% buffer B at a flow rate of 500 nl/min. A voltage of 3.0 kV was applied for electrospray ionization. Dynamic exclusion was employed with 120 s exclusion and a 2.0 Th mass window. MS1 and MS2 were acquired in the Orbitrap with nominal resolving power of 7500 at 400 *m/z*. Isolation was performed in the linear ion trap in data-dependent mode on the top ten peaks following each MS1 with 1.0 Th isolation width. Fragmentation was performed in the higher-energy collisional dissociation cell with stepped collision energies of 32, 38, and 44%. Raw spectra were converted to mzml files using MSConvert (122) for analysis by

FragPipe. The MS/MS spectra obtained from higher-energy collisional dissociation fragmentation in the Orbitrap were identified, and TMT intensities were integrated in FragPipe (123, 124), against the UniProt 07/11/2021 human proteome release (longest entry for each protein group) with 20,429 proteins plus reverse sequences and common contaminants, with a maximum peptide-level FDR of 0.01. Cysteine alkylation (+57.02146 Da) and TMT modification (+229.1629 on lysine and N termini) were set as fixed modifications, and half-tryptic cleavages were allowed. Keratins, nonhuman contaminants, and immunoglobulins were filtered from proteins lists. For lysate and pellet experiments, integrated intensities at the protein level for each channel were normalized to the median intensity of that channel at the peptide level, and then p values were moderated (125). For immunoprecipitation, p values were generated based on our previously reported bait–prey correlation method (54). Local FDRs (q values) were assessed using Storey's modification of the method of Benjamini and Hochberg (55, 56). The Storey π_0 factor was 1.0 for lysate and pellet experiments and 0.13 for the affinity purification followed by MS experiment.

Data availability

MS-based proteomics raw data and search results are available at the PRIDE Archive at PXD033498. Quantitation is available in Tables S1–S3.

Supporting information—This article contains supporting information.

Acknowledgments—We thank E. Yeh for the Ub^{HA} plasmid, A. Ting for the ^{cyt}APEX2 plasmid, J. Sanes for the $^{ER}HRP^{N175S}$ plasmid, and T. Yamamoto for the pX330A-1x2 plasmid. Support was provided by the University of California.

Author contributions—J. C. G. conceptualization; M. F. E., M. M. S., Z. L., and J. C. G. methodology; K. K. N. validation; M. F. E., K. K. N., G. M. Q., and J. C. G. formal analysis; M. F. E., K. K. N., M. M. S., G. M. Q., M. R. M., and J. C. G. investigation; M. F. E. and J. C. G. writing–original draft; K. K. N. writing–review & editing; J. C. G. visualization; J. C. G. supervision; J. C. G. project administration.

Conflict of interest—The authors declare that they have no conflicts of interest with the contents of this article.

Abbreviations—The abbreviations used are: A1AT, alpha-1 antitrypsin; APEX, ascorbate peroxidase; BiP, binding immunoglobulin protein; cDNA, complementary DNA; CHO, Chinese hamster ovary cell line; DMEM, dulbecco's modified eagle's medium; DSP, dithiobis(succinimidyl propionate); eGFP, enhanced GFP; ER, endoplasmic reticulum; ERAD, ER-associated degradation; FC, fold change; FDR, false discovery rate; ^{Flag}TTR, Flag-tagged TTR; HEK293T, human embryonic kidney 239T cell line; HRP, horseradish peroxidase; Hsp, heat shock protein; $Hspa13^{Flag}$, Hspa13 with a C-terminal Flag; MS, mass spectrometry; NBD, nucleotide-binding domain; NEFM, neurofilament medium chain; OST, oligosaccharyltransferase; RIPA, radioimmunoprecipitation assay; RRID, research resource identifier; SBD, substrate-binding domain; SRP, signal recognition particle; TBS, tris-buffered saline; Tg, thapsigargin; TMT, tandem mass tag; TTR, transthyretin; Ub_{HA}, hemagglutinin-tagged ubiquitin; UPR, unfolded protein response.

References

1. Ellgaard, L., and Helenius, A. (2003) Quality control in the endoplasmic reticulum. *Nat. Rev. Mol. Cell Biol.* **4**, 181–191
2. Owji, H., Nezafat, N., Negahdaripour, M., Hajiebrahimi, A., and Ghasemi, Y. (2018) A comprehensive review of signal peptides: structure, roles, and applications. *Eur. J. Cell Biol.* **97**, 422–441
3. Juszkiewicz, S., and Hegde, R. S. (2018) Quality control of orphaned proteins. *Mol. Cell* **71**, 443–457
4. Hegde, R. S., and Zavodszky, E. (2019) Recognition and degradation of mislocalized proteins in health and disease. *Cold Spring Harb. Perspect. Biol.* **11**, a033902
5. Zhang, X., and Shan, S. O. (2014) Fidelity of cotranslational protein targeting by the signal recognition particle. *Annu. Rev. Biophys.* **43**, 381–408
6. Jomaa, A., Gamerdinger, M., Hsieh, H.-H., Wallisch, A., Chandrasekaran, V., Ulusoy, Z., *et al.* (2022) Mechanism of signal sequence handover from NAC to SRP on ribosomes during ER-protein targeting. *Science* **375**, 839–844
7. Guo, H., Sun, J., Li, X., Xiong, Y., Wang, H., Shu, H., *et al.* (2018) Positive charge in the n-region of the signal peptide contributes to efficient post-translational translocation of small secretory preproteins. *J. Biol. Chem.* **293**, 1899–1907
8. Johnson, N., Haßdenteufel, S., Theis, M., Paton, A. W., Paton, J. C., Zimmermann, R., *et al.* (2013) The signal sequence influences post-translational ER translocation at distinct stages. *PLoS One* **8**, e75394
9. Hessa, T., Sharma, A., Mariappan, M., Eshleman, H. D., Gutierrez, E., and Hegde, R. S. (2011) Protein targeting and degradation are coupled for elimination of mislocalized proteins. *Nature* **475**, 394–397
10. Rodrigo-Brenni, M. C., Gutierrez, E., and Hegde, R. S. (2014) Cytosolic quality control of mislocalized proteins requires RNF126 recruitment to Bag6. *Mol. Cell* **55**, 227–237
11. Lang, S., Pfeffer, S., Lee, P. H., Cavalie, A., Helms, V., Forster, F., *et al.* (2017) An update on Sec61 channel functions, mechanisms, and related diseases. *Front. Physiol.* **8**, 887
12. Ziska, A., Tatzelt, J., Dudek, J., Paton, A. W., Paton, J. C., Zimmermann, R., *et al.* (2019) The signal peptide plus a cluster of positive charges in prion protein dictate chaperone-mediated Sec61 channel gating. *Biol. Open* **8**, bio040691
13. Matlack, K. E. S., Misselwitz, B., Plath, K., and Rapoport, T. A. (1999) BiP acts as a molecular ratchet during posttranslational transport of prepro-α factor across the ER membrane. *Cell* **97**, 553–564
14. Linxweiler, M., Schick, B., and Zimmermann, R. (2017) Let's talk about Secs: sec61, Sec62 and Sec63 in signal transduction, oncology and personalized medicine. *Signal Transduct. Target. Ther.* **2**, 17002
15. Schorr, S., Nguyen, D., Haßdenteufel, S., Nagaraj, N., Cavalié, A., Greiner, M., *et al.* (2020) Identification of signal peptide features for substrate specificity in human Sec62/Sec63-dependent ER protein import. *FEBS J.* **287**, 4612–4640
16. Lang, S., Benedix, J., Fedeles, S. V., Schorr, S., Schirra, C., Schäuble, N., *et al.* (2012) Differential effects of Sec61α-, Sec62- and Sec63-depletion on transport of polypeptides into the endoplasmic reticulum of mammalian cells. *J. Cell Sci.* **125**, 1958–1969
17. Ruiz-Canada, C., Kelleher, D. J., and Gilmore, R. (2009) Cotranslational and posttranslational N-glycosylation of polypeptides by distinct mammalian OST isoforms. *Cell* **136**, 272–283
18. Braunger, K., Pfeffer, S., Shrimal, S., Gilmore, R., Berninghausen, O., Mandon, E. C., *et al.* (2018) Structural basis for coupling protein transport and N-glycosylation at the mammalian endoplasmic reticulum. *Science* **360**, 215–219
19. Go, C. D., Knight, J. D. R., Rajasekharan, A., Rathod, B., Hesketh, G. G., Abe, K. T., *et al.* (2021) A proximity-dependent biotinylation map of a human cell. *Nature* **595**, 120–124
20. Estoppey, D., Lee, C. M., Janoschke, M., Lee, B. H., Wan, K. F., Dong, H., *et al.* (2017) The natural product cavinafungin selectively interferes with

zika and dengue virus replication by inhibition of the host signal peptidase. *Cell Rep.* **19**, 451–460
21. Grizenkova, J., Akhtar, S., Hummerich, H., Tomlinson, A., Asante, E. A., Wenborn, A., *et al.* (2012) Overexpression of the Hspa13 (Stch) gene reduces prion disease incubation time in mice. *Proc. Natl. Acad. Sci. U. S. A.* **109**, 13722–13727
22. Rane, N. S., Kang, S.-W., Chakrabarti, O., Feigenbaum, L., and Hegde, R. S. (2008) Reduced translocation of nascent prion protein during ER stress contributes to neurodegeneration. *Dev. Cell* **15**, 359–370
23. Rane, N. S., Chakrabarti, O., Feigenbaum, L., and Hegde, R. S. (2010) Signal sequence insufficiency contributes to neurodegeneration caused by transmembrane prion protein. *J. Cell Biol.* **188**, 515–526
24. Mookherjee, D., Majumder, P., Mukherjee, R., Chatterjee, D., Kaul, Z., Das, S., *et al.* (2019) Cytosolic aggregates in presence of non-translocated proteins perturb endoplasmic reticulum structure and dynamics. *Traffic* **20**, 943–960
25. Mayer, M. P. (2013) Hsp70 chaperone dynamics and molecular mechanism. *Trends Biochem. Sci.* **38**, 507–514
26. Hartl, F. U., Martin, J., and Neupert, W. (1992) Protein folding in the cell: the role of molecular chaperones Hsp70 and Hsp60. *Annu. Rev. Biophys. Biomol. Struct.* **21**, 293–322
27. Rosenzweig, R., Nillegoda, N. B., Mayer, M. P., and Bukau, B. (2019) The Hsp70 chaperone network. *Nat. Rev. Mol. Cell Biol.* **20**, 665–680
28. Clerico, E. M., Tilitsky, J. M., Meng, W., and Gierasch, L. M. (2015) How Hsp70 molecular machines interact with their substrates to mediate diverse physiological functions. *J. Mol. Biol.* **427**, 1575–1588
29. Otterson, G. A., Flynn, G. C., Kratzke, R. A., Coxon, A., Johnston, P. G., and Kaye, F. J. (1994) Stch encodes the "ATPase core" of a microsomal stress 70 protein. *EMBO J.* **13**, 1216–1225
30. Otterson, G. A., and Kaye, F. J. (1997) A "core ATPase", Hsp70-like structure is conserved human, rat, C. elegans STCH proteins. *Gene* **199**, 287–292
31. Marchler-Bauer, A., Bo, Y., Han, L., He, J., Lanczycki, C. J., Lu, S., *et al.* (2017) CDD/SPARCLE: functional classification of proteins via subfamily domain architectures. *Nucleic Acids Res.* **45**, D200–D203
32. Shoulders, M. D., Ryno, L. M., Genereux, J. C., Moresco, J. J., Tu, P. G., Wu, C., *et al.* (2013) Stress-independent activation of XBP1s and/or ATF6 reveals three functionally diverse ER proteostasis environments. *Cell Rep.* **3**, 1279–1292
33. Grandjean, J. M. D., Madhavan, A., Cech, L., Seguinot, B. O., Paxman, R. J., Smith, E., *et al.* (2020) Pharmacologic IRE1/XBP1s activation confers targeted ER proteostasis reprogramming. *Nat. Chem. Biol.* **16**, 1052–1061
34. Aoki, M., Yamamoto, K., Ohyama, S., Yamamura, Y., Takenoshita, S., Sugano, K., *et al.* (2005) A genetic variant in the gene encoding the stress70 protein chaperone family member STCH is associated with gastric cancer in the Japanese population. *Biochem. Biophys. Res. Commun.* **335**, 566–574
35. Yamagata, N., Furuno, K., Sonoda, M., Sugimura, H., and Yamamoto, K. (2008) Stomach cancer-derived del223V-226L mutation of the STCH gene causes loss of sensitization to TRAIL-mediated apoptosis. *Biochem. Biophys. Res. Commun.* **376**, 499–503
36. Bakhos-Douaihy, D., Seaayfan, E., Demaretz, S., Komhoff, M., and Laghmani, K. (2021) Differential effects of STCH and stress-inducible Hsp70 on the stability and maturation of NKCC2. *Int. J. Mol. Sci.* **22**, 2207
37. He, Y., Xu, R., Zhai, B., Fang, Y., Hou, C., Xing, C., *et al.* (2020) Hspa13 promotes plasma cell production and antibody secretion. *Front. Immunol.* **11**, 913
38. Zhai, B., Liu, X., Xu, Y., Zhu, G., Zhou, S., He, Y., *et al.* (2022) Single-cell atlas of splenocytes reveals a critical role of a novel plasma cell−specific marker Hspa13 in antibody class-switching recombination and somatic hypermutation. *Mol. Immunol.* **141**, 79–86
39. Gao, C., Deng, J., Zhang, H., Li, X., Gu, S., Zheng, M., *et al.* (2021) HSPA13 facilitates NF-κB−mediated transcription and attenuates cell death responses in TNFα signaling. *Sci. Adv.* **7**, eabh1756
40. Hurshman, A. R., White, J. T., Powers, E. T., and Kelly, J. W. (2004) Transthyretin aggregation under partially denaturing conditions is a downhill polymerization. *Biochemistry* **43**, 7365–7381
41. Sekijima, Y., Wiseman, R. L., Matteson, J., Hammarström, P., Miller, S. R., Sawkar, A. R., *et al.* (2005) The biological and chemical basis for tissue-selective amyloid disease. *Cell* **121**, 73–85
42. Christianson, J. C., Olzmann, J. A., Shaler, T. A., Sowa, M. E., Bennett, E. J., Richter, C. M., *et al.* (2011) Defining human ERAD networks through an integrative mapping strategy. *Nat. Cell Biol.* **14**, 93–105
43. Li, X., Song, Y., Sanders, C. R., and Buxbaum, J. N. (2016) Transthyretin suppresses amyloid-β secretion by interfering with processing of the amyloid-β protein precursor. *J. Alzheimers Dis.* **52**, 1263–1275
44. Kadowaki, H., Nagai, A., Maruyama, T., Takami, Y., Satrimafitrah, P., Kato, H., *et al.* (2015) Pre-emptive quality control protects the ER from protein overload via the proximity of ERAD components and SRP. *Cell Rep.* **13**, 944–956
45. Kadowaki, H., Satrimafitrah, P., Takami, Y., and Nishitoh, H. (2018) Molecular mechanism of ER stress-induced pre-emptive quality control involving association of the translocon, Derlin-1, and HRD1. *Sci. Rep.* **8**, 1–11
46. Lyu, Z., Sycks, M. M., Espinoza, M. F., Nguyen, K. K., Montoya, M. R., Galapate, C. M., *et al.* (2022) Monitoring protein import into the endoplasmic reticulum in living cells with proximity labeling. *ACS Chem. Biol.* **17**, 1963–1977
47. Sato, T., Sako, Y., Sho, M., Momohara, M., Suico, M. A., Shuto, T., *et al.* (2012) STT3B-dependent posttranslational N-glycosylation as a surveillance system for secretory protein. *Mol. Cell* **47**, 99–110
48. Holden, P., and Horton, W. A. (2009) Crude subcellular fractionation of cultured mammalian cell lines. *BMC Res. Notes* **2**, 243
49. Chakrabarti, O., and Hegde, R. S. (2009) Functional depletion of mahogunin by cytosolically exposed prion protein contributes to neurodegeneration. *Cell* **137**, 1136–1147
50. Joesch, M., Mankus, D., Yamagata, M., Shahbazi, A., Schalek, R., Suissa-Peleg, A., *et al.* (2016) Reconstruction of genetically identified neurons imaged by serial-section electron microscopy. *Elife* **5**, e15015
51. Lam, S. S., Martell, J. D., Kamer, K. J., Deerinck, T. J., Ellisman, M. H., Mootha, V. K., *et al.* (2015) Directed evolution of APEX2 for electron microscopy and proximity labeling. *Nat. Methods* **12**, 51–54
52. Tan, Y. L., Genereux, J. C., Pankow, S., Aerts, J. M., Yates, J. R., and Kelly, J. W. (2014) ERdj3 is an endoplasmic reticulum degradation factor for mutant glucocerebrosidase variants linked to Gaucher's disease. *Chem. Biol.* **21**, 967–976
53. Wang, B., Heath-Engel, H., Zhang, D., Nguyen, N., Thomas, D. Y., Hanrahan, J. W., *et al.* (2008) BAP31 interacts with Sec61 translocons and promotes retrotranslocation of CFTRΔF508 via the derlin-1 complex. *Cell* **133**, 1080–1092
54. Mei, L., Montoya, M. R., Quanrud, G. M., Tran, M., Villa-Sharma, A., Huang, M., *et al.* (2020) Bait correlation improves interactor identification by tandem mass tag-affinity purification-mass spectrometry. *J. Proteome Res.* **19**, 1565–1573
55. Storey, J. D., and Tibshirani, R. (2003) Statistical significance for genomewide studies. *Proc. Natl. Acad. Sci. U. S. A.* **100**, 9440–9445
56. Benjamini, Y., and Hochberg, Y. (1995) Controlling the false discovery rate - a practical and powerful approach to multiple testing. *J. R. Stat. Soc. Ser. B Stat. Methodol.* **57**, 289–300
57. Ting, L., Rad, R., Gygi, S. P., and Haas, W. (2011) MS3 eliminates ratio distortion in isobaric multiplexed quantitative proteomics. *Nat. Methods* **8**, 937–940
58. Ast, T., Michaelis, S., and Schuldiner, M. (2016) The protease Ste24 clears clogged translocons. *Cell* **164**, 103–114
59. Kayatekin, C., Amasino, A., Gaglia, G., Flannick, J., Bonner, J. M., Fanning, S., *et al.* (2018) Translocon declogger Ste24 protects against IAPP oligomer-induced proteotoxicity. *Cell* **173**, 62–73.e9
60. Harada, Y., Ohkawa, Y., Kizuka, Y., and Taniguchi, N. (2019) Oligosaccharyltransferase: a gatekeeper of health and tumor progression. *Int. J. Mol. Sci.* **20**, 6074

61. Pfeffer, S., Dudek, J., Schaffer, M., Ng, B. G., Albert, S., Plitzko, J. M., *et al.* (2017) Dissecting the molecular organization of the translocon-associated protein complex. *Nat. Commun.* **8**, 14516
62. Lee, S., Shin, Y., Kim, K., Song, Y., Kim, Y., and Kang, S.-W. (2020) Protein translocation acquires substrate selectivity through ER stress-induced reassembly of translocon auxiliary components. *Cells* **9**, 518
63. Fons, R. D., Bogert, B. A., and Hegde, R. S. (2003) Substrate-specific function of the translocon-associated protein complex during translocation across the ER membrane. *J. Cell Biol.* **160**, 529–539
64. Alexander, E. J., Ghanbari Niaki, A., Zhang, T., Sarkar, J., Liu, Y., Nirujogi, R. S., *et al.* (2018) Ubiquilin 2 modulates ALS/FTD-linked FUS-RNA complex dynamics and stress granule formation. *Proc. Natl. Acad. Sci. U. S. A.* **115**, E11485–E11494
65. Kaye, F. J., Modi, S., Ivanovska, I., Koonin, E. V., Thress, K., Kubo, A., *et al.* (2000) A family of ubiquitin-like proteins binds the ATPase domain of Hsp70-like Stch. *FEBS Lett.* **467**, 348–355
66. Dejgaard, K., Theberge, J.-F., Heath-Engel, H., Chevet, E., Tremblay, M. L., and Thomas, D. Y. (2010) Organization of the Sec61 translocon, studied by high resolution native electrophoresis. *J. Proteome Res.* **9**, 1763–1771
67. Guo, F., and Snapp, E. L. (2013) ERdj3 regulates BiP occupancy in living cells. *J. Cell Sci.* **126**, 1429–1439
68. Pobre, K. F. R., Poet, G. J., and Hendershot, L. M. (2019) The endoplasmic reticulum (ER) chaperone BiP is a master regulator of ER functions: getting by with a little help from ERdj friends. *J. Biol. Chem.* **294**, 2098–2108
69. Sun, M., Kotler, J. L. M., Liu, S., and Street, T. O. (2019) The endoplasmic reticulum (ER) chaperones BiP and Grp94 selectively associate when BiP is in the ADP conformation. *J. Biol. Chem.* **294**, 6387–6396
70. Shelkovnikova, T. A., Robinson, H. K., Connor-Robson, N., and Buchman, V. L. (2013) Recruitment into stress granules prevents irreversible aggregation of FUS protein mislocalized to the cytoplasm. *Cell Cycle* **12**, 3383–3391
71. Chen, J. J., Genereux, J. C., Qu, S., Hulleman, J. D., Shoulders, M. D., and Wiseman, R. L. (2014) ATF6 activation reduces the secretion and extracellular aggregation of destabilized variants of an amyloidogenic protein. *Chem. Biol.* **21**, 1564–1574
72. Colon, W., and Kelly, J. W. (1992) Partial denaturation of transthyretin is sufficient for amyloid fibril formation *in vitro*. *Biochemistry* **31**, 8654–8660
73. Kong, K.-Y. E., Coelho, J. P. L., Feige, M. J., and Khmelinskii, A. (2021) Quality control of mislocalized and orphan proteins. *Exp. Cell Res.* **403**, 112617
74. Costa, G. da, Gomes, R. A., Guerreiro, A., Mateus, É., Monteiro, E., Barroso, E., *et al.* (2011) Beyond genetic factors in familial amyloidotic polyneuropathy: protein glycation and the loss of fibrinogen's chaperone activity. *PLoS One* **6**, e24850
75. Goldsteins, G., Andersson, K., Olofsson, A., Dacklin, I., Edvinsson, Å., Baranov, V., *et al.* (1997) Characterization of two highly amyloidogenic mutants of transthyretin. *Biochemistry* **36**, 5346–5352
76. Kamitani, T., Kito, K., Nguyen, H. P., and Yeh, E. T. H. (1997) Characterization of NEDD8, a developmentally down-regulated ubiquitin-like protein. *J. Biol. Chem.* **272**, 28557–28562
77. Hammarström, P., Sekijima, Y., White, J. T., Wiseman, R. L., Lim, A., Costello, C. E., *et al.* (2003) D18G transthyretin is monomeric, aggregation prone, and not detectable in plasma and cerebrospinal fluid: a prescription for central nervous system amyloidosis? *Biochemistry* **42**, 6656–6663
78. Susuki, S., Sato, T., Miyata, M., Momohara, M., Suico, M. A., Shuto, T., *et al.* (2009) The endoplasmic reticulum-associated degradation of transthyretin variants is negatively regulated by BiP in mammalian cells. *J. Biol. Chem.* **284**, 8312–8321
79. Chen, J. J., Genereux, J. C., Suh, E. H., Vartabedian, V. F., Rius, B., Qu, S., *et al.* (2016) Endoplasmic reticulum proteostasis influences the oligomeric state of an amyloidogenic protein secreted from mammalian cells. *Cell Chem. Biol.* **23**, 1282–1293
80. Flynn, G. C., Chappell, T. G., and Rothman, J. E. (1989) Peptide binding and release by proteins implicated as catalysts of protein assembly. *Science* **245**, 385–390
81. Gaut, J. R., and Hendershot, L. M. (1993) Mutations within the nucleotide binding site of immunoglobulin-binding protein inhibit ATPase activity and interfere with release of immunoglobulin heavy chain. *J. Biol. Chem.* **268**, 7248–7255
82. McCarty, J. S., and Walker, G. C. (1991) DnaK as a thermometer: threonine-199 is site of autophosphorylation and is critical for ATPase activity. *Proc. Natl. Acad. Sci. U. S. A.* **88**, 9513–9517
83. O'Brien, M. C., Flaherty, K. M., and McKay, D. B. (1996) Lysine 71 of the chaperone protein Hsc70 is essential for ATP hydrolysis. *J. Biol. Chem.* **271**, 15874–15878
84. Barthel, T. K., Zhang, J., and Walker, G. C. (2001) ATPase-defective derivatives of Escherichia coli DnaK that behave differently with respect to ATP-induced conformational change and peptide release. *J. Bacteriol.* **183**, 5482–5490
85. Daniels, R., Kurowski, B., Johnson, A. E., and Hebert, D. N. (2003) N-linked glycans direct the cotranslational folding pathway of influenza hemagglutinin. *Mol. Cell* **11**, 79–90
86. Chen, X., VanValkenburgh, C., Liang, H., Fang, H., and Green, N. (2001) Signal peptidase and oligosaccharyltransferase interact in a sequential and dependent manner within the endoplasmic reticulum. *J. Biol. Chem.* **276**, 2411–2416
87. Rutkowski, D. T., Ott, C. M., Polansky, J. R., and Lingappa, V. R. (2003) Signal sequences initiate the pathway of maturation in the endoplasmic reticulum lumen. *J. Biol. Chem.* **278**, 30365–30372
88. Genereux, J. C., Qu, S., Zhou, M., Ryno, L. M., Wang, S., Shoulders, M. D., *et al.* (2015) Unfolded protein response-induced ERdj3 secretion links ER stress to extracellular proteostasis. *EMBO J.* **34**, 4–19
89. Mezgarzadeh, J. S., Romine, I. C., Smith-Cohen, E. M., Grandjean, J. M., Kelly, J. W., Genereux, J. C., *et al.* (2022) ATF6 activation reduces amyloidogenic transthyretin secretion through increased interactions with endoplasmic reticulum proteostasis factors. *Cells* **11**, 1661
90. Rabouille, C. (2017) Pathways of unconventional protein secretion. *Trends Cell Biol.* **27**, 230–240
91. Volkmar, N., Fenech, E., and Christianson, J. C. (2016) New MAPS for misfolded proteins. *Nat. Cell Biol.* **18**, 724–726
92. Lee, J.-G., Takahama, S., Zhang, G., Tomarev, S. I., and Ye, Y. (2016) Unconventional secretion of misfolded proteins promotes adaptation to proteasome dysfunction in mammalian cells. *Nat. Cell Biol.* **18**, 765–776
93. Gettins, P. G. W. (2002) Serpin structure, mechanism, and function. *Chem. Rev.* **102**, 4751–4804
94. Tsutsui, Y., Dela Cruz, R., and Wintrode, P. L. (2012) Folding mechanism of the metastable serpin α_1-antitrypsin. *Proc. Natl. Acad. Sci. U. S. A.* **109**, 4467–4472
95. Strnad, P., McElvaney, N. G., and Lomas, D. A. (2020) Alpha$_1$-antitrypsin deficiency. *N. Engl. J. Med.* **382**, 1443–1455
96. Nguyen, D., Stutz, R., Schorr, S., Lang, S., Pfeffer, S., Freeze, H. H., *et al.* (2018) Proteomics reveals signal peptide features determining the client specificity in human TRAP-dependent ER protein import. *Nat. Commun.* **9**, 3765
97. Voorhees, R. M., and Hegde, R. S. (2016) Structure of the Sec61 channel opened by a signal sequence. *Science* **351**, 88–91
98. Nilsson, I., Lara, P., Hessa, T., Johnson, A. E., von Heijne, G., and Karamyshev, A. L. (2015) The code for directing proteins for translocation across ER membrane: SRP cotranslationally recognizes specific features of a signal sequence. *J. Mol. Biol.* **427**, 1191–1201
99. Patschull, A. O. M., Segu, L., Nyon, M. P., Lomas, D. A., Nobeli, I., Barrett, T. E., *et al.* (2011) Therapeutic target-site variability in α_1-antitrypsin characterized at high resolution. *Acta Crystallogr. F Struct. Biol. Cryst. Commun.* **67**, 1492–1497
100. McCarthy, C., Saldova, R., Wormald, M. R., Rudd, P. M., McElvaney, N. G., and Reeves, E. P. (2014) The role and importance of glycosylation of acute phase proteins with focus on alpha-1 antitrypsin in acute and chronic inflammatory conditions. *J. Proteome Res.* **13**, 3131–3143

101. Sakuma, T., Nishikawa, A., Kume, S., Chayama, K., and Yamamoto, T. (2014) Multiplex genome engineering in human cells using all-in-one CRISPR/Cas9 vector system. *Sci. Rep.* **4**, 5400
102. Mollereau, B., Manié, S., and Napoletano, F. (2014) Getting the better of ER stress. *J. Cell Commun. Signal* **8**, 311–321
103. Quanrud, G. M., Montoya, M. R., Mei, L., Awad, M. R., and Genereux, J. C. (2021) Hsp40 affinity to identify proteins destabilized by cellular toxicant exposure. *Anal. Chem.* **93**, 16940–16946
104. Yuan, A., Rao, M. V., Veeranna, and Nixon, R. A. (2017) Neurofilaments and neurofilament proteins in health and disease. *Cold Spring Harb. Perspect. Biol.* **9**, a018309
105. Rane, N. S., Yonkovich, J. L., and Hegde, R. S. (2004) Protection from cytosolic prion protein toxicity by modulation of protein translocation. *EMBO J.* **23**, 4550–4559
106. Cui, J., Chen, W., Sun, J., Guo, H., Madley, R., Xiong, Y., *et al.* (2015) Competitive inhibition of the endoplasmic reticulum signal peptidase by non-cleavable mutant preprotein cargos. *J. Biol. Chem.* **290**, 28131–28140
107. Guo, H., Xiong, Y., Witkowski, P., Cui, J., Wang, L., Sun, J., *et al.* (2014) Inefficient translocation of preproinsulin contributes to pancreatic β cell failure and late-onset diabetes. *J. Biol. Chem.* **289**, 16290–16302
108. Huttlin, E. L., Bruckner, R. J., Navarrete-Perea, J., Cannon, J. R., Baltier, K., Gebreab, F., *et al.* (2021) Dual proteome-scale networks reveal cell-specific remodeling of the human interactome. *Cell* **184**, 3022–3040.e28
109. Schweppe, D. K., Huttlin, E. L., Harper, J. W., and Gygi, S. P. (2018) BioPlex display: an interactive suite for large-scale AP–MS protein–protein interaction data. *J. Proteome Res.* **17**, 722–726
110. Brown, C. A., Schmidt, C., Poulter, M., Hummerich, H., Klohn, P. C., Jat, P., *et al.* (2014) *In vitro* screen of prion disease susceptibility genes using the scrapie cell assay. *Hum. Mol. Genet.* **23**, 5102–5108
111. Kityk, R., Kopp, J., and Mayer, M. P. (2018) Molecular mechanism of J-domain-triggered ATP hydrolysis by Hsp70 chaperones. *Mol. Cell* **69**, 227–237.e4
112. Hassdenteufel, S., Johnson, N., Paton, A. W., Paton, J. C., High, S., and Zimmermann, R. (2018) Chaperone-mediated Sec61 channel gating during ER import of small precursor proteins overcomes Sec61 inhibitor-reinforced energy barrier. *Cell Rep.* **23**, 1373–1386
113. Sundaram, A., Plumb, R., Appathurai, S., and Mariappan, M. (2017) The Sec61 translocon limits IRE1alpha signaling during the unfolded protein response. *Elife* **6**, e27187
114. [preprint] Sun, S., Li, X., and Mariappan, M. (2022) Signal sequences encode information for protein folding in the endoplasmic reticulum. *bioRxiv*. https://doi.org/10.1101/2020.06.04.133884
115. Snapp, E. L., Reinhart, G. A., Bogert, B. A., Lippincott-Schwartz, J., and Hegde, R. S. (2004) The organization of engaged and quiescent translocons in the endoplasmic reticulum of mammalian cells. *J. Cell Biol.* **164**, 997–1007
116. Schnell, D. J., and Hebert, D. N. (2003) Protein translocons. *Cell* **112**, 491–505
117. Phoomak, C., Cui, W., Hayman, T. J., Yu, S.-H., Zhao, P., Wells, L., *et al.* (2021) The translocon-associated protein (TRAP) complex regulates quality control of N-linked glycosylation during ER stress. *Sci. Adv.* **7**, eabc6364
118. Klock, H. E., and Lesley, S. A. (2009) The polymerase incomplete primer extension (PIPE) method applied to high-throughput cloning and site-directed mutagenesis. *Methods Mol. Biol.* **498**, 91–103
119. Hung, V., Udeshi, N. D., Lam, S. S., Loh, K. H., Cox, K. J., Pedram, K., *et al.* (2016) Spatially resolved proteomic mapping in living cells with the engineered peroxidase APEX2. *Nat. Protoc.* **11**, 456–475
120. Lee, S. Y., Kang, M. G., Park, J. S., Lee, G., Ting, A. Y., and Rhee, H. W. (2016) APEX fingerprinting reveals the subcellular localization of proteins of interest. *Cell Rep.* **15**, 1837–1847
121. Washburn, M. P., Wolters, D., and Yates, J. R. (2001) Large-scale analysis of the yeast proteome by multidimensional protein identification technology. *Nat. Biotechnol.* **19**, 242–247
122. Chambers, M. C., Maclean, B., Burke, R., Amodei, D., Ruderman, D. L., Neumann, S., *et al.* (2012) A cross-platform toolkit for mass spectrometry and proteomics. *Nat. Biotechnol.* **30**, 918–920
123. Kong, A. T., Leprevost, F. V., Avtonomov, D. M., Mellacheruvu, D., and Nesvizhskii, A. I. (2017) MSFragger: ultrafast and comprehensive peptide identification in mass spectrometry–based proteomics. *Nat. Methods* **14**, 513–520
124. da Veiga Leprevost, F., Haynes, S. E., Avtonomov, D. M., Chang, H.-Y., Shanmugam, A. K., Mellacheruvu, D., *et al.* (2020) Philosopher: a versatile toolkit for shotgun proteomics data analysis. *Nat. Methods* **17**, 869–870
125. Kammers, K., Cole, R. N., Tiengwe, C., and Ruczinski, I. (2015) Detecting significant changes in protein abundance. *EuPA Open Proteom.* **7**, 11–19